

Keng H. Hsu

| | | |
|---|---|---------------------|
| Objective | Faculty position with research focus in Nano-/Micro-technology and Renewable Energy | |
| Education | <i>University of Illinois at Urbana-Champaign, IL</i> | 2004-2009 |
| | Ph.D. in Mechanical Engineering Dissertation "Harnessing Solid-State Ionic Transport for Nanomanufacturing and Nanodevices" | |
| | <i>National Taiwan University of Science & Technology, Taipei, Taiwan</i> | 1998-2000 |
| | M.S. in Mechanical Engineering Thesis "A Study of Application of Miniaturized Thermal Conductivity Detector in Gas Concentration Determination" | |
| | <i>National Taiwan University of Science & Technology, Taipei, Taiwan</i> | 1994-1998 |
| | B.A. in Mechanical Engineering GPA: 3.8 | |
| Research & Teaching Experience | <i>University of Illinois at Urbana-Champaign, IL</i> | 2009-present |
| | Postdoctoral Research Fellow (Research advisors: Nicholas Fang, Placid Ferreira) <ul style="list-style-type: none">▪ <i>Solid-State Superionic Stamping patterning technology, S4</i><ul style="list-style-type: none">○ Construct an S4 machine○ Develop supporting systems for meter-scale large-area patterning with the S4 technique○ Develop computational interface for process control and monitoring○ Develop complementary fabrication techniques for S4-based dielectric patterning▪ <i>Renewable Energy</i><ul style="list-style-type: none">○ Design, fabricate, and characterize Si nanowire-based solar cells○ Design, fabricate, and characterize Si nanowire-based battery anodes○ Fabricate 1D, 2D silicon nanostructure-based thermoelectric devices○ Develop computational models for battery electrode-electrolyte interface kinetics and transport▪ <i>Metallic nanostructure enabled bio-sensing</i><ul style="list-style-type: none">○ Design, construct, and characterize plasmonic DNA sensors○ Design, fabricate, and characterize novel Raman and Fluorescence sensors | |
| | <i>University of Illinois at Urbana-Champaign, IL</i> | 2005-2009 |
| | Research Assistant (Advisors: Nicholas Fang, Placid Ferreira) <ul style="list-style-type: none">▪ <i>Solid-State Superionic Stamping patterning technology, S4</i><ul style="list-style-type: none">○ Develop a novel all-solid, ambient condition, direct metal nanopatterning technique○ Develop computational model transport and kinetics of solid electrolyte-metal systems○ Characterize electrochemical properties of solid electrolyte-metal systems▪ <i>Micro-/Nano-fabrication</i><ul style="list-style-type: none">○ Design and implement novel micro-/nano-manufacturing techniques○ Design, fabricate, and characterize metallic nanostructure-based plasmonic device○ Fabricate novel optical devices utilizing conventional lithographic processes▪ <i>Metallic nanostructure enabled bio-sensing</i><ul style="list-style-type: none">○ Fabricate and characterize plasmonic structures○ Characterize optical properties of fabricated devices | |
| | <i>University of Illinois at Urbana-Champaign, IL</i> | 2005 |
| | Teaching Assistant <ul style="list-style-type: none">▪ Course: Introduction to gas dynamics | |

Experimental Fabrication

& Computational Expertise

- Lithography processes
- Scanning-probe based nanofabrication
- Solid electrochemical nanofabrication
- Conventional machining

Characterization

- Electron Microscopy
- Scanning Probe Microscopy / Spectroscopy
- Raman Spectroscopy / Fluorescence Spectroscopy
- Fluorescence Correlation Spectroscopy
- Electro-Impedance Spectroscopy
- Cyclic / linear voltammetry
- Chrono-amperometry / -potentiometry

Computation

- Finite Element Modeling
- Finite Difference Time Domain

Journal Publication

Peer-reviewed journal papers

- Keng Hsu, Peter Schultz, Placid Ferreira, and Nicholas Fang, "Electrochemical Nanoimprinting with Solid-State Superionic Stamps," *Nano Letters*, 2007, Vol. 7 No. 2, 446-451
- Keng Hsu, Peter Schultz, Placid Ferreira, and Nicholas X. Fang, "Exploiting transport of guest metal ions in a host ionic crystal lattice for nanofabrication: Cu nanopatterning with Ag₂S," *Applied Physics A*, Volume 97, Issue 4 (2009), Page 863
- Keng Hsu, Ju H. Back, Moonsub Shim, Kin H. Fung, Placid Ferreira, and Nicholas Fang, "SERS EM-field Enhancement Study through Fast Raman Mapping of Optical Sierpinski Carpet Fractals," *Journal of Raman Spectroscopy*, DOI: 10.1002/jrs. 2581, 2010
- Keng Hsu, Placid Ferreira, and Nicholas Fang, "Numerical Modeling for the Dynamic Balance Between Interfacial Kinetics and Ionic Transport of Ag-Ag₂S systems," *Solid State Ionics*, Submitted, 2010
- Keng Hsu, Placid Ferreira, and Nicholas Fang, "Controlled Directional Growth of Silver Micro Wires on a Solid Electrolyte Surface," *Applied Physics Letters*, 96, 024101, 2010
- Keng Hsu, Peter Schultz, Placid Ferreira, and Nicholas X. Fang, "Electrochemical Nanoimprinting of Silver and Copper with the Solid-State Superionic Stamping (S4) Process," *Soft Lithography*, John Rogers and Hong H. Lee (ed.), John Wiley and Sons, 2008.
- Winston Chern, Keng Hsu, Ik Su Chun, Bruno Pavanelli De Azeredo, Nick Fang, Placid Ferreira, and Xiuling Li, "Non-Lithographic Patterning and Metal-Assisted Chemical Etching for Manufacturing of Tunable Light-Emitting Silicon Nanowire Arrays," *Nature Nanotech*, submitted, 2009
- S. Choi, M. Yan, I. Adesida, K. Hsu, and N. Fang, "Ultradense gold nanostructures fabricated using hydrogen silsesquioxane resist and applications for surface-enhanced Raman spectroscopy," *J. Vac. Sci. Technol.* B 27 (6), 2009, 2640-2643.
- Chaturvedi P., K. Hsu, S. Zhang, and N. X. Fang, "New Frontiers of Metamaterials: Design and Fabrication," *MRS Bulletin*, 33:10, 915-920, 2008
- Schultz P., Hsu, K., Fang, N., and Ferreira, P., "Solid-state electrochemical nanoimprinting of copper," *Journal of Vacuum Science & Technology B: Microelectronics and Nanometer Structures* -- November 2007 -- Volume 25, Issue 6, pp. 2419-2424
- Y. E. Wu, K. Chen, C. W. Chen and K. Hsu, "Fabrication and characterization of thermal conductivity detectors (TCDs) of different flow channel and heater designs," *Sensors and Actuators A: Physical*, Vol 100, 1, 2002, 37- 45.
- Keng Hsu, Placid Ferreira, and Nicholas Fang, "Direct Nanopatterning With Solid Ionic Stamping," *IMECE2006-13441 Proceedings of IMECE2006 2006 ASME International Mechanical Engineering Congress and Exposition*, Nov. 2006, Chicago, Illinois USA

Patent Application

- N. Fang, K. Hsu, K. Rapaka, and P. Ferreira, "Pattern transfer by Solid-State Electrochemical Stamping," *US patent application*, No. 11/376,908.
- K. Jacobs, K. Hsu, N. Fang, P. Ferreira, "Direct Nanoscale Patterning of Metals Using Polymer Electrolytes," *US patent application*, No. TF07168-US
- X. Li, N. Fang, P. Ferreira, W. Chern, I. S. Chun, K. Hsu, "Method of Forming an Array of High Aspect Ratio Semiconductor Nanostructures," No. TF09098-pro

Publicity

Technical Presentations

- "Solid State Electrochemical Nanoimprint," *2007 MRS Spring Meeting*, San Francisco, CA, Apr. 2007
- "Direct Electrochemical Nanopatterning With Solid Ionic Conductors," *211th Meeting of the Electrochemical Society* Chicago, IL, May 2007
- "A Solid Phase Electrochemical Nanoimprint Process," *Fifth international conference on nanoimprint and nanoprint technology*, San Francisco, CA, Nov. 2006
- "Active nanopatterning with solid state ionic conduction," *2006 NSF Design, Service, and Manufacturing Grantees and Research Conference*, St. Louis, MO, July 2006
- "Direct Nanopatterning with Solid Ionic Stamping," *ASME international mechanical engineering congress and exposition*, Chicago, IL, Nov. 2006

News Releases

- U of I now: New stamping process creates metallic interconnects, nanostructures (<http://www.news.uiuc.edu/news/07/0221superionic.html>)
- Nanotechnology Today: New stamping process creates metallic interconnects, nanostructures (<http://nanotechnologytoday.blogspot.com/2007/02/metallic-interconnects-nanostructures.html>)
- Eurekalert.com : New stamping process creates metallic interconnects, nanostructures (http://www.eurekalert.org/pub_releases/2007-02/uoia-nsp022107.php)
- Science Daily: New Stamping Process Creates Metallic Interconnects, Nanostructures (<http://www.sciencedaily.com/releases/2007/02/070222160011.htm>)

Other Professional Experience

Five Pioneers Mechanical Engineering, Taipei, Taiwan

2002-2004

Beverage Process/Production Design Engineer

- Beverage production line / equipment design
- Overseeing production line installation
- Business proposal

References

- Assistant Professor Nicholas X. Fang** Department of Mechanical Engineering
University of Illinois at Urbana-Champaign
4414 Mechanical Engineering Laboratory
1206 West Green Street, Urbana, IL
217.265.8262 / nicfang@illinois.edu
- Professor Placid M. Ferreira** Department of Mechanical Engineering
University of Illinois at Urbana-Champaign
148 Mechanical Engineering Building
1206 West Green Street, Urbana, IL
217.333.0639 / pferreira@illinois.edu
- Assistant Professor John E. Wentz** School of Engineering
University of St. Thomas
2115 Summit Ave., St. Paul, MN
651.962.5413 / john.wentz@stthomas.edu
- Mr. Scott J. Robinson** Beckman Institute
University of Illinois at Urbana-Champaign
405 North Mathews Ave., Urbana, IL
217.265.5071 / sjrobin@illinois.edu
- Professor William P. King** Department of Mechanical Engineering
University of Illinois at Urbana-Champaign
4409 Mechanical Engineering Laboratory
1206 West Green Street, Urbana, IL
217.244.3864 / wpk@illinois.edu

INTRODUCTION

The unique nature of ionic transport is not only the origin of a large number of physical and chemical phenomena but it is also this coupled mass-charge transport that is the core of a wide range of applications such as manufacturing, energy conversion, and sensing techniques. The materials in which ionic transport can take place are not only limited to traditional liquid electrolytes, but have been extended to polymer, glass, as well as crystalline solids as depicted in [Figure 1](#). Sharing the same coupled mass-charge transport properties with their liquid counterpart, solid-state ionic materials have gained numerous interests in their transport properties and the discovery of new materials that exhibit this coupled mass-charge transport phenomenon since the 1890's when Nernst discovered the ionic transport in refractory oxides. Not until a few decades ago has research effort begun to take advantage of this unique property for applications in areas such as high performance batteries, fuel and electrolysis cells, chemical sensors, as well as thermoelectric converters [1-3].

More recently, several physical phenomena that are coupled with this unique transport in solid electrolytes have started to strike curiosity in understanding them and raise interests in exploiting them to develop novel applications. Some examples includes the dissolution of metal on its interface with a solid electrolyte, the-order-of-magnitude increase in electrical conductivity while a junction is bridged by an ionic species, the plasmonic properties of tiny metal clusters formed while solid electrolytes interact with electromagnetic waves or electric fields, and the thermal energy carried by ionic species

while migrating through a solid ionic crystal [4-25]. These interesting phenomena not only deserve in depth study on their physical nature, but have potential in revolutionizing the field of nanopatterning, transistors, sensing and actuation, and energy conversion with the enhancement of these properties at nano-scale.

With the thorough investigations and understandings in the kinetics of a metal-solid electrolyte interface, there has only been very little work on developing a patterning technique that is based on controlled corrosion of metal on its interface with a solid electrolyte. Similar to its liquid counterpart whose electrolytic behavior has long been exploited for electrochemical machining, solid electrolytes have the same ability to dissolve metal substrate upon contacting a metallic surface whose electron potential is altered. Superior to liquid electrolytes whose flow can affect electrical current distribution and can cause non-uniform etching of materials, solid electrolytes are ideal candidates for stamping-type of patterning due to its structural integrity. One of the main goals of this research work is to develop a stamping-type patterning technique based on the controlled dissolution of metal on a metal-solid electrolyte interface and the coupled charge-mass transport in the solid electrolyte. This approach has high potential in creating a new patterning technique that will revolutionize micro-/nano-patterning of metal.

The ability to precisely control dimension and geometry of metallic features finds favor in the field of plasmonics because the core of such phenomenon lies in the interaction between sub-wavelength noble metal particles such as Ag with excitation electromagnetic waves. The study of Surface Plasmons Polaritons (SPP) and Localized Surface Plasmons

Resonance (LSPR) has recently received a renewed interest because of its vast potential in applications such as nano-optics and sub-diffraction imaging. Among them, sensing schemes based on emissive processes such as Surface Enhanced Raman Scattering, SERS, and Metal Enhanced Fluorescence, MEF, have received an explosion of research efforts put into them for the past few decades. The reasoning lies in the fact that with relatively straightforward instrumentation a small collection of molecules can be identified. While lab-scaled demonstration of SERS-/MEF-based sensing of physical, chemical, and biological quantities have continuously grown in number, the understanding of what is believed to be the origin of the electromagnetic-field enhancement has been limited. Studies carried out both theoretically and experimentally are usually based on simple geometry such as spheres and disks [26-28]. Despite of the advances in numerical tools, the understanding of enhancement effects provided by complex geometries has been hampered by the limitations of current manufacturing techniques in the geometry control and resolution. A new nanopatterning technique that offers solution to these issues will open up the door to a new array of studies that provide both experimental and theoretical insights by enabling experimental verification of theoretical predictions.

In fulfilling the need for faster electronics, numerous achievements in the field of nanoelectronics have been made for the past few decades in light of the new properties materials exhibit at nanoscale. An example is the quantized conductance of metal nanowires that is seen when dimension of the metal wire is close to the Fermi wavelength of the electrons transmitting through the nanowires; under this condition, the ballistic nature of the electron transport give rise to a higher conductance than its bulk form.

Conventionally, fabricating metallic nano-scale metallic wires and junctions has relied on lithographic methods and liquid state electrolytic growth control which are expensive, difficult, and not environmental friendly. Finding a new way of producing nanometer junctions in a reversible manner to either complement or replace existing methods is the key to taking the full advantage of the use of nano-junctions for constructing integrated electronics and nano-scale devices. As another main goal of this research work, the methodology of using solid electrolyte to generate nano-scale metallic wires and junctions will be explored.

In addressing the issues above, the theme of this dissertation is developed. As illustrated in [Figure 2](#), a direct metal nanopatterning technique will be developed to address limitations of current fabrication techniques. This developed direct metal patterning technique will be used to fabricate plasmonic features with resonance in the optical range to demonstrate its applications in Surface Enhanced Raman Scattering as well as Metal Enhanced Fluorescence. In addition, a novel approach to constructing micro-/nano-metal wires in a controlled manner will be described. Its application in constructing break-junction devices will also be demonstrates.

ORGANIZATION OF DISSERTATION

The different aspects of the author's research efforts will be divided into 6 chapters. While each chapter will have its comprehensive introduction, experimental, and results and discussion sections, all chapters revolve around the theme of harnessing solid-state ionic transport for nanomanufacturing and nanodevices. Chapter 1 will describe the new solid-state electrochemical fabrication approach, Solid State Superionic Stamping, S4, developed as a result of the author's research effort. Chapter 2 will discuss the extent of such an approach to heterogeneous systems such as silver sulfide and copper. Chapter 3 will describe the new numerical model developed to understand, and help design and optimize the new patterning approach described in chapter 1. Chapter 4 will be dedicated to the use of S4 and the development of a new characterization approach to study plasmon-enhanced emissive processes such as Raman scattering and fluorescence emission. A case study will be carried out in Chapter 5 to examine the relations between the farfield extinction and local electromagnetic field of a given plasmonic feature. This relation will be discussed in the context of the EM-field enhancement of the plasmonic feature for Raman scattering and fluorescence. Chapter 6 will present the novel approach, developed in the author's research effort, to construct break-junction devices through controlled growth of metal wires on solid electrolyte surfaces. The theoretical support by the model described in chapter 3 will also be provided.

FIGURES

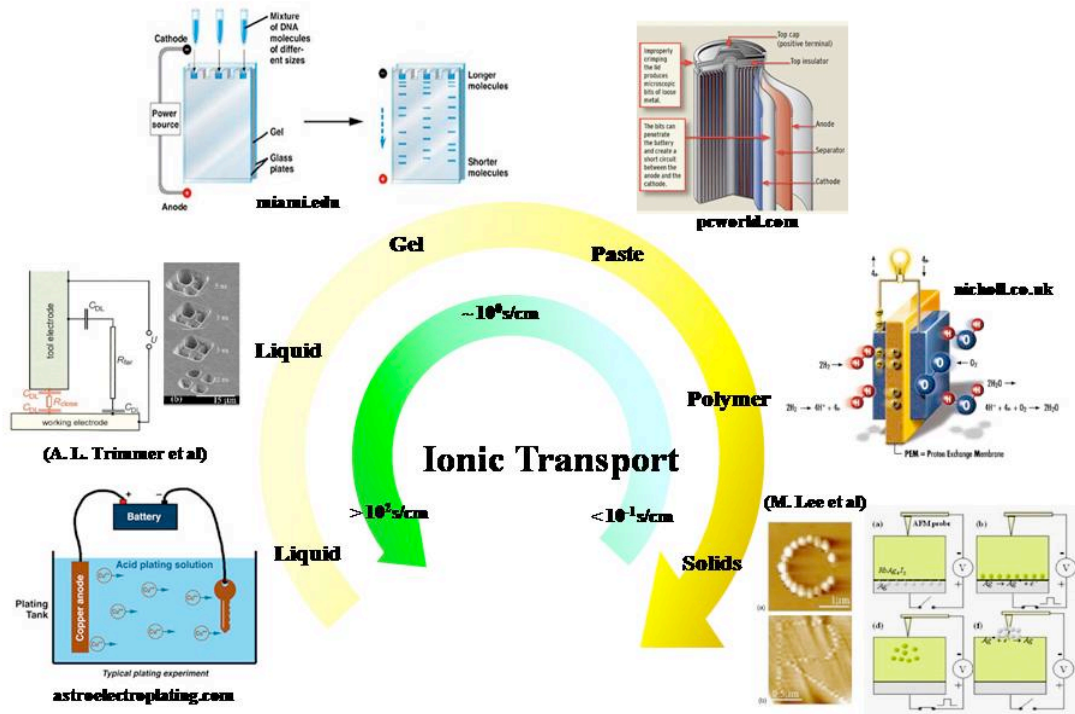


Figure 1 Applications of ionic transport

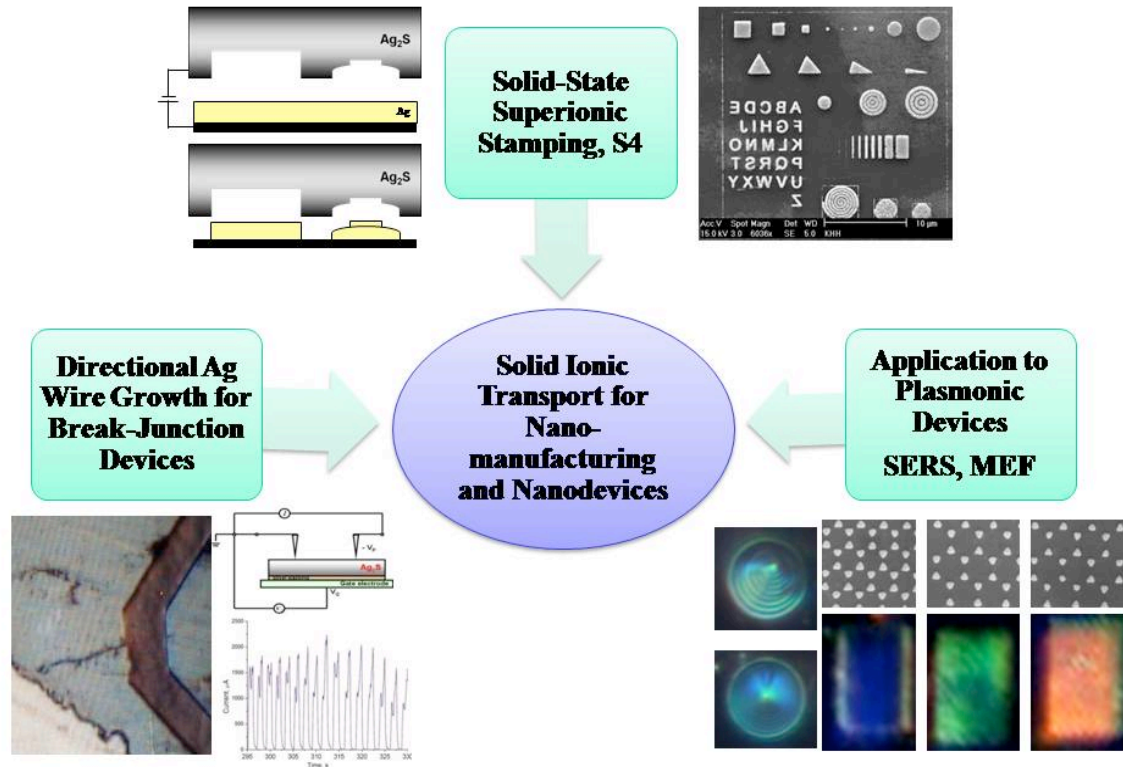


Figure 2 Aspects of research work described in this dissertation

REFERENCES

1. W. van Gool et al., Annual Review of Materials Science 1974, 4:3, 311-335
2. P. McGeehin et al., Review Fast ion conduction materials, Journal of Materials Science 12 (1977) 1-27
3. H. Rickert, Solid Ionic Conductors: Principle and Applications, Angew. Chem. Int. Ed. Engl. 17, 37-4
4. R. Schuster, V. Kirchner, X. H. Xia, A. M. Bittner, G. Ertl, Nanoscale Electrochemistry, Phys. Rev. Lett. 80, 5599 (1998).
5. P. Avouris, T. Hertel, R., Appl. Phys. Lett. 71, 285 (1997).
6. Terabe et al., Applied physics letters, Vol. 80, No. 21 2002.
7. Terabe et al., Journal of applied physics, Vol. 91, No. 12 2002.
8. F. Prinz, et al, App. Phy. Letters, Vol 85, No. 16, 2004.
9. R. D. Armstrong, T. Dickinson, and P. M. Willis, Electroanal. Chem. And Interfac. Electrochem., 57(1974)231.
10. Krans J M et al., Nature, 1995, 375
11. Muller et al., Phys. Rev. B, 1996, 53, 1022-1025

12. Van Ruitenbeek J M et al., Rev. Sci. Instrum., 1996, 67, 108
13. Landman U et al., Phys. Rev. Lett., 1996, 77, 1362
14. Pascual J I et al., Science, 1995, 267 1793
15. Rubio G et al., Phys. Rev. Lett., 1996, 76 2302
16. Snow E S et al., Appl. Phys. Lett., 1996, 69 269
17. Li C Z et al., Appl. Phys. Lett., 1998, 72 894
18. Li C Z et al., Nanotechnology, 10 (1999), 221-223
19. F. Q. Hie et al., Phs. Rev. Lett., 93, NO. 12, 2004, 128303-1 128303-4
20. Shunuchi Kaeriyama et al., IEEE Journal of Solid State Cirtuits, Vol. 40 NO. 1, 2005, 168-176
21. K. Terabe et al., Nature, Vol. 433, 6, 2005, 47-50
22. Eftekhari, Analytical Letters, 2001, 34, 1087-1095
23. K. Terabe et al., Journal of Applied Physics, 2002, Vol. 91, NO. 12, 10110-10114
24. K. Terabe et al., Applied Physics Letters, 2002, Vol. 80, NO. 21, 4009-4011.
25. K. Terabe et al., Small, 2005, NO. 10, 971-975
26. McFarland AD, Young MA, Dieringer JA, Van Duyne RP., J. Phys. Chem. B 109:11279–85, 2005
27. A. Baca, J. Montgomery, S. Gray, J. Rogers, Appl. Phys. Lett. 94, 243109, 2009
28. M. Stewart, C. Anderton, L. Thompson, J. Maria, S. Gray, J. Rogers, R. Nuzzo , Chem, Rev., 108, 494-521, 2008

CHAPTER 1.

**SOLID IONIC TRANSPORT BASED
NANOMANUFACTURING:
SOLID-STATE SUPERIONIC STAMPING, S4**

1.1 INTRODUCTION

Patterning nanoscale metallic features is an integral part of a wide variety of fabrication applications including nano-electronic, photonic and nano-electromechanical devices, as well as nanoscale chemical sensors and transducers[1,2]. However, the common practice for generating metallic patterns has relied on an indirect approach; nanoscale patterns are first created on photoresist by optical lithography or by mechanical imprinting[3,4,5], and followed by metal deposition and the subsequent lift-off or etching processes. The damascene process pursued by the semiconductor industry, for instance, deposits the copper interconnects electrochemically into the trenches of patterned dielectrics and uses chemical mechanical polishing to remove excess metal in an expensive, complex, multi-step process that requires stringent process environment control and very costly equipment. An alternative method, electrochemical micromachining (ECM), has been proposed to directly produce sub-micron metallic features[6,7]. However, significant limitations on lateral extension of the features are associated with electrochemical machining due to a considerable diffusion length of the reacting species. Accelerated etching at sharp edges and corners also leads to low geometrical fidelity in the pattern transferred from the electrochemical tool to substrate surface[6]. In addition, the use of

liquids might contaminate both the tool and the substrate.

In this chapter, we address the above disadvantages by introducing a solid state electrochemical imprinting process that directly creates high resolution metallic nanopatterns in a single step. The proposed process, coined as Solid-State Superionic Stamping (or S4), is schematically presented in [Figure 1.1](#). At the core of this process is a solid electrolyte or superionic conductor[8] that is widely used in battery and fuel cells due to its excellent ionic conductivity at room and relatively low temperatures. A stamp made of a superionic conductor with a mobile cation (silver sulfide, for example, in which the silver ions are mobile), is pre-patterned with fine features and brought into contact with the metallic substrate to be patterned. On the application of an electrical bias with the substrate as anode and a metallic electrode at the back of the stamp as cathode, a solid state electrochemical reaction takes place at the contact points of the interface. At the anode-electrolyte interface, an appreciable potential drop causes the oxidation of silver atoms on the substrate and produces mobile silver ions. These mobilized ions migrate across the interface and through the interstitial channels and defect network in the lattice of the superionic conductor towards the cathode, until they recombine with electrons. The anodic dissolution progressively removes a metallic layer of the substrate at the contact area with the stamp. Assisted by a nominal pressure to maintain electrical contact, the stamp progresses into the substrate generating a shape complementary to the pre-patterned features on it. The advantage of using solid-state superionic conductors is that mass transport is restricted to the physical contact between the patterned electrolyte and the substrate (the anode), making it an ideal tool for nanoscale pattern transfer with high fidelity.

This method is clearly distinguished from scanning probe-based electrochemical patterning methods, in which the high spatial resolution stems from limited diffusion of the electrolyte ions[9] or geometrically confined liquid electrolyte volume[10]. The mobility of ions in an array of solid electrolytes, such as Ag_2S and RbAg_4I_5 has been exploited to create nanostructures in “direct write” like processes. Sub-hundred nanometer line and dot patterns have been written using scanning probe microscopy[11,12]. These techniques use an electric potential applied across a scanning probe and a solid electrolyte substrate surface to induce the migration of metal ions from within the substrate to the vicinity of the probe to form metallic clusters to create lines or dots on the electrolyte surface[13]. The practicality of this direct pattern writing as a manufacturing process is limited because of low throughput, difficulties in dimensional control of the structures formed and processing parameters (the stand-off distance of the probe must be precisely regulated and its travel speed must be coordinated to the growth of the structure. Most importantly, the metal structures are embedded on the electrolyte surface making their subsequent use in many applications difficult.

1.2 RESULTS AND DISCUSSION

We validate the concept of the S4 process through the use of silver sulfide as the solid-state superionic stamp for electrochemically imprinting silver nanoscale features, as shown in [Figure 1.2](#). First, to prepare a silver sulfide stamp, we started with synthesizing a dense silver sulfide pellet in an improvised furnace with programmable temperature control. Sulfur powder with 99.999% purity (from Fisher Scientific Company) was hand

pressed into a 3-mm diameter pellet and inserted into a glass tube (3mm internal diameter) with a silver pellet (from Kurt J. Lesker company). The two were then held together with a small constant force (required for a dense silver sulfide pellet) provided by a spring. The assembly was placed in the furnace at 400°C for 10 hours to allow formation and annealing of silver sulfide. The silver sulfide pellets created in this manner were characterized with x-ray diffraction (Rigaku D-Max System with a scanning range (2- θ) from 0 to 60 degrees and a scan rate of 1.5 degrees per minute) and compared with standard peaks for the powder form beta-silver sulfide. Characterization of a number of pellets confirmed the composition of the silver sulfide pellets and the consistent output of the above process. The synthesized silver pellets were machined to a conical tip at one end. This end was planarized to produce a flat mesa of 300 μ m in diameter for stamping. The patterns on the stamp, such as those shown in [Figure 1.2\(a\)](#), were produced by focused ion-beam milling (FEI Dual-Beam DB-235) with a 50pA ion current at a milling rate of 50nm/min. The deepest trench of the stamp in [Figure 1.2\(a\)](#) was about 250nm. We also demonstrated direct embossing of the silver sulfide stamps against silicon molds.

For different patterning experiments, a number of silver substrates were prepared by electron beam evaporation onto a 300- μ m thick glass cover slip cleaned using RCA1 solution. The silver films were deposited over a 10 nm Cr seed layer at a chamber pressure of 5×10^{-6} torr and a stable rate of 0.1nm/s. To perform stamping, the glass substrate with the silver film was then mounted on a glass window and a single-axis micro-actuator was used for feeding the stamp down to the substrate. The stamp was attached to this assembly via an elastomer that provides 48MPa of pressure at 20% compressive strain uniformly across the actual contact area between the electrode and the

silver substrate. This nominal pressure (well below the yield stress of silver sulfide) ensured a consistent contact between the stamp and the substrate during the progress of electrochemical imprinting.

The electrical potential for electrochemical imprinting is controlled by a digital potentiostat (Gamry Instrument Model Reference 600) with a blocking electrode attached to the stamp as the cathode and the silver substrate being patterned as the anode. The process was performed in the chronoamperometry mode of the potentiostat in which the potential between anode and cathode was kept constant while the current was monitored. To produce the results shown in [Figure 1.2b](#), electrochemical imprinting was performed with a driving potential of 0.8V on a 250nm-thick silver film. Close-up views in the bottom panels confirm that all designed geometrical features with dimensions greater than 80nm were successfully transferred with dimensional deviations from the stamp being less than 10nm. The lateral resolution achieved is 100nm for line width (as observed in the line pattern) and 80nm for line spacing (in the concentric-ring pattern).

A remarkable feature of the S4 process, in contrast to the liquid-based electrochemical etching, is the capability of reproducing acute angles. As seen in [Figure 1.2a and 1.2c](#), even the triangle with a 15° angle was transferred with fine details at the tip (radius of curvature of 50nm). This unique capability is essential for plasmonic devices and sensors that require a sharp geometric singularity for effective and controllable enhancement of optical near field, such as Surface Enhanced Raman Scattering (SERS). In addition, solid state electrochemical imprinting offers excellent pattern transfer fidelity. Our measurement indicate that the mismatch between the feature size on the stamp and that of the formed complementary pattern on silver substrate is less than 10nm, only about one-

tenth of what can be achieved in liquid state electrochemical machining, even with nanosecond pulse methods to constraint field diffusion[7]. Improving the pattern transfer fidelity through optimization of the process parameters such as the applied bias, contact pressure is one of our ongoing efforts.

One can also observe in [Figure 1.2b](#) that the surface and edges of the transferred silver pattern appear to be relatively rough as compared to the exposed Cr surface. This can be attributed to an insufficient relief depth on the silver sulfide stamp made by FIB patterning, resulting undesired contact between the relieved stamp surfaces. The resulting dissolution at these undesired contact surfaces coupled with the use of relatively high electrical bias (0.8V) that increases the rate of nucleation and growth of pores on the metal surface explains the relatively rough surfaces. In addition, during intermediate etch steps and after extended etching, it is also typical to observe silver clusters tens of nanometers in diameter and height dispersed on the Cr surface, even though such features are not noticeable on the polished stamp surface. These are thought to have originated from the nucleation-growth-of-hole nature[14] of the silver electrode dissolution. A detailed study of the mechanical and chemical conditions of the contacts at the stamp-metal interface and their impact on the patterning will be addressed in our future work.

To verify the electrochemical activity, we also performed a set of anodic sweep experiments between the stamp and 250nm thick silver substrate (the anode) with scan range from 0 to 0.5V at a speed of 20mV/s ([Figure 1.3a](#)). A distinct peak in total current is observed between 0.1V and 0.2V as the applied bias is increased, associated to anodic dissolution of silver by breaking the space charge layer at the silver/electrolyte interface and the acceleration of this process with increasing bias. Further increasing the bias,

however, does not accompany the increased current density at the anode, due to the finite rate of migration of silver ions in the stamp. In consequence, the silver ions resulting from dissolution accumulate at the vicinity of the interface, giving rise to a concentration overpotential that counteracts with the applied potential, decreasing the dissolution rate. As the anodic bias keeps increasing, the concentration overpotential resulting from the increased silver ion flux also increases and blocks the ionic flux from the dissolving interface, causing a drop of current density until about 0.26V applied bias. This characteristic hump curve in the forward voltage sweep is clearly distinguished from the anodic sweeping curve measured from a blocking electrode made of carbon, which simply indicates the Ohmic response of electronic conductivity of Ag_2S (a typical n-type semiconductor). The difference between the two curves in [Figure 1-3a](#) clearly indicates the ionic interaction between the silver substrate and the stamp.

We present in [Figure 1.3b](#) the total current evolution during the electrochemical etching process, obtained when using new or unused Ag_2S stamps at different voltages to etch a 250nm thick silver film. Currents for the different voltage levels follow a similar trend: they ramp up to their highest value with activation of the electrochemical reaction, slope down to lower values in the second stage as polarization of the stamp increases and reach a steady state as the etching progresses. Finally, the current decreases sharply as a result of the depletion of silver at the anode, and stabilizes with a low but nonzero value (that corresponds to the electronic conduction, as Ag_2S is a mixed conductor), indicating a completion of the process. This depletion of silver is verified by observations from the back side of the optically transparent glass substrate. Except for 0.2V bias which did not etch through the thickness of the film, we integrated the areas under different current

curves, and found the total charge transferred (about 3.9×10^{-3} Coulomb) is nearly equal for the different applied biases. This is interesting because the volume of silver dissolved in the different trials is nearly equal. Taking the product of applied bias and the total charge transferred, and normalizing it by the amount of silver removed, our estimate shows a specific energy of 500kJ/kg, for the electrochemical imprinting of silver using a typical Ag_2S stamp. Based on the above observation, we can also estimate an average etch rate for an unpolarized (unused) silver stamp to be 1.28, 2.0, 3.16nm/s for applied biases of 0.4, 0.6, and 0.8V, respectively.

In addition, [Figure 1.3c](#) shows the temporal profile of etch current of a single stamp that has been stored for a few days prior to performing 9 repetitions of stamping process on different area of an 80nm thick silver film with 0.3V bias, and a 30-second interval between each stamping. The same current profile as described previously is also observed for each run repetition. Except for the first two runs, the total charge transferred is nearly constant. We have observed that the first two runs did not etch a complete pattern through the film, and suspect that this is due to an oxidation layer formed on the silver sulfide stamp. Over the 9 repetitions of stamping, we have also observed the current profile to have evolved into having slightly extended etching time and lower peak current as the current profile eventually settles down to a stable shape.

To demonstrate the fine resolution of the S4 process, in [Figure 1.4](#) we performed an etching experiment with amorphous silver layer coated onto borosilicate glass (samples from Arrandee™). To obtain the 3D etch profile of the fine features from electrochemical imprinting, we conducted contact-mode Atomic Force Microscopy (AFM) measurements on a Digital Instrument Multimode system with an ultra sharp

probe (20 degree tip angle, 10nm tip radius) from MikroMasch. The samples are scanned with in 1umx1um windows (corresponding to the dotted white lines in the upper panel) at a scan rate of 0.5Hz. Both AFM and SEM measurements indicate that the smallest line width and spacing of 5nm were transferred faithfully, reaching the resolution limit of the focused ion beam tool used for preparing the stamp. Also seen in the SEM micrograph of [Figure 1.4](#) (top panel) is the apparent improvement in the surface roughness of the top surfaces of the pattern and the silver residue at the bottom. Such improved surface roughness is likely due to the nucleation controlled anode dissolution at low overpotential conditions.

We also studied the process rates of a polarized stamp at steady state on a 470nm silver film substrate (amorphous silver layer coated onto borosilicate glass, samples from ArrandeeTM) with a driving potential of 0.3V. Electrochemical etching or stamping was performed for varying amounts of time and the corresponding etch depths were measured using an AFM. As shown in [Figure 1.5](#), the silver removal/etch rate throughout the process was found to remain constant at 4nm/s. Remarkably, we obtained higher process rates than we had seen with new stamps on evaporated silver films. Further, a constant stamping rate implies constant ionic conductivity of silver sulfide, in spite of the increase in silver concentration change, or the composition change of the silver sulfide stamp.

This is in good agreement with Hebb[15] and Wagner's[16] electrochemical measurements of β -phase silver sulfide (most stable at room temperature), which suggest that ionic conductivity of this phase is almost independent of composition within its stoichiometric range, because the lattice structure of β -phase silver sulfide is quite open and is considerably rich in interstitial channels for motion and sites for residence of silver

ions.

By assuming the Ag₂S stamp was of ideal stoichiometry at the beginning of electrochemical reaction, we estimated the concentration of excessive silver absorbed into the stamp by calculating the amount of silver being oxidized and the affected volume of the stamp. The silver ion mass transport in the stamp is governed by the Nernst-Planck equation⁸ relating the transient concentration change to the chemical diffusion and electrochemical migration of the species in the stamp. For the time interval required to completely deplete the silver substrate, a characteristic diffusion layer thickness (proportional to the square root of the overpotential and the time wherein the bias was applied) is estimated to be around 500µm. The total volume of silver removed was then calculated [17] to be approximately $4 \times 10^{-11} \text{ m}^3$. As a result, at the end of one stamping operation, the local concentration of excessive silver ion in the diffusion-affected volume was estimated to change from 0 to 90 moles/m³, or the stoichiometry ratio from 2 to 2.0017[18], which is still in the stoichiometric range of ionically conductive β-phase silver sulfide.

1.3 CONCLUSION

In conclusion, the S4 process offers a simple and robust approach to manufacturing metallic nanostructures at 50 nm resolution. The process works under ambient environmental conditions and does not require complex process steps or expensive equipment. The process rates and repeatability are surprisingly high (considering the rudimentary equipment and chemicals used, and the fact that no process optimization was

performed), and the S4 process can easily be scaled up for high-throughput production. Further, given the room temperature operation, low voltages and highly-localized nature of the transport phenomena exploited, we expect S4 to perform as an energy-efficient process. For the experiments reported here, the patterns were directly inscribed into the stamps using focused ion-beam milling. However, given the good ductility of silver sulfide, stamp patterns could readily be produced by embossing with a hard master, leading to considerably more favorable process economics.

The exploitation of fast ionic conduction in solids as a manufacturing technique to produce high resolution nanostructures, as exemplified by the S4 process, represents a new, efficient and cost-effective avenue for current processes. While this letter has described patterning in silver with silver sulfide stamps, the process is not restricted to these materials. We have successfully patterned copper with similar results and consistency. For patterning metal structures, we will explore a variety of other ionic conductors such as Na^+ , Cu^+ , Pb^{2+} superionic conductors, solid polymer electrolytes and glasses.

1.4 FIGURES

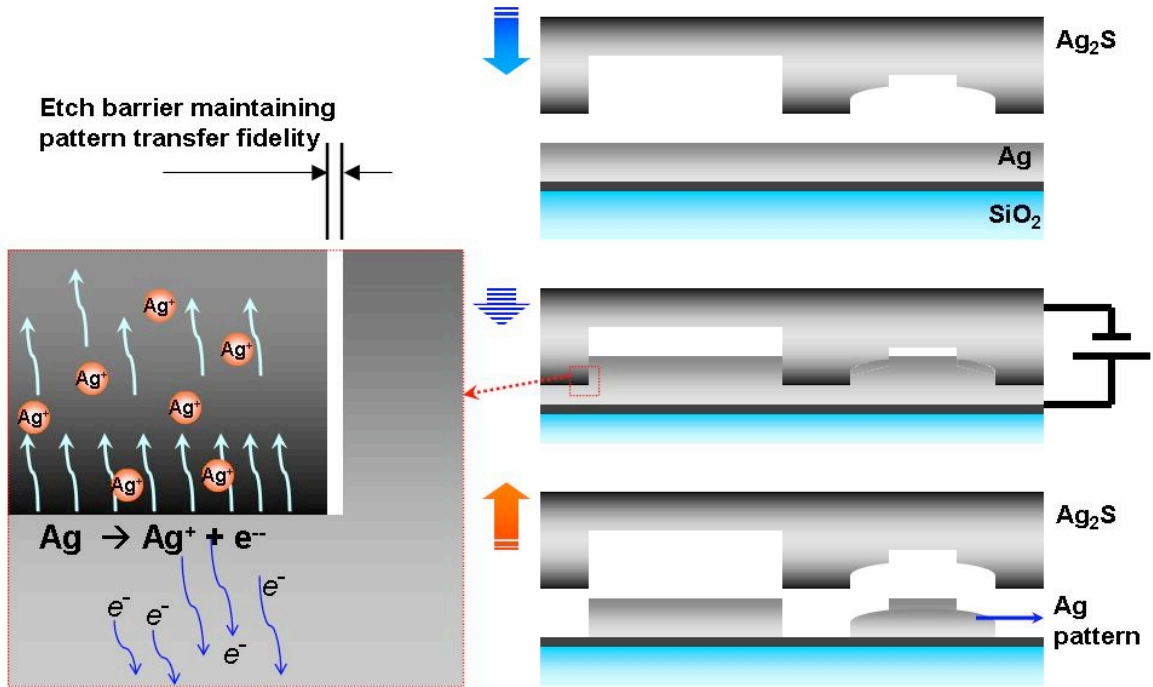


Figure 1.1 Schematic of the Solid-State Superionic Stamping process. A stamp made of a solid ionic conductor is brought into contact with the workpiece or substrate to be patterned. A biasing electrical potential dissolves the metal at the workpiece(anode)-stamp interface. (a) To initiate solid state ionic stamping, a pre-patterned solid electrolyte (silver sulfide in our work) backed with an inert metal is connected to a potentiostat as the counter electrode (cathode) and the metal substrate to be patterned is the anode. (b) The pre-patterned solid electrolyte stamp is placed in contact with the metal workpiece or substrate and, with an applied voltage bias and nominal force, electrochemical etching takes place at the contact areas progressively dissolving metal into the solid ionic stamp and engraving the workpiece. (c) Electrochemical imprinting is completed, resulting in a pattern on the metal substrate complementary to that on the solid electrolyte stamp.

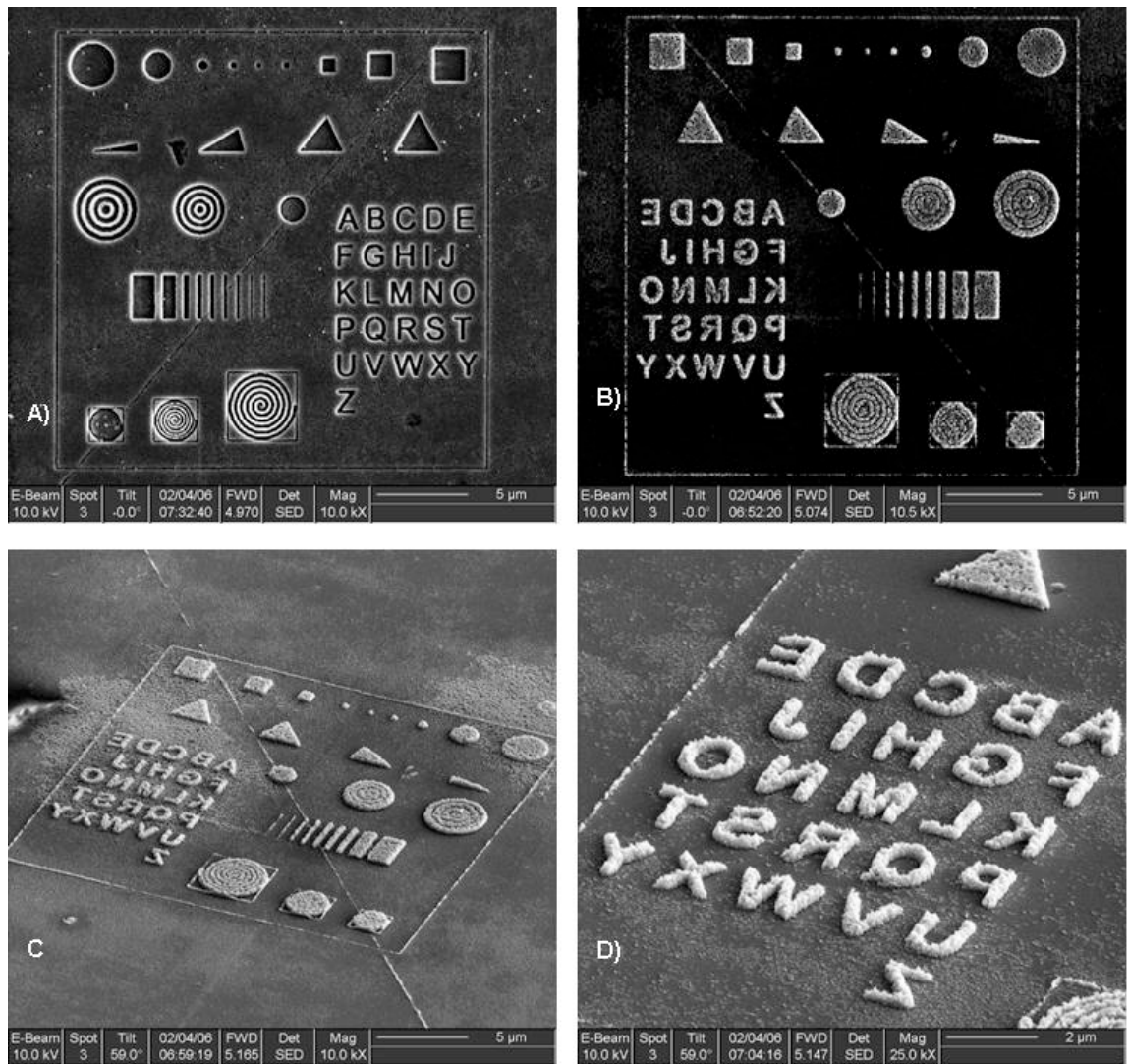


Figure 1.2 An example of silver patterning using the S4 process. (a) A FIB patterned Ag_2S stamp with an array of geometric patterns and letters. The radius of the circles range from 2.4 μm to 200 nm; the squares are patterned with a range of width from 300 nm to 1.7 μm ; the triangles are patterned with varying angles from 15° to 60° with 15° steps, and the radius of the acute corner is as small as 50 nm. Each of the concentric rings is made with uniform pitch, from left to right the pitch measures 500 nm, 390 nm and 240 nm, respectively. The rectangles are patterned with a width varying from 60 nm to 1.3 μm . To form the letters, the linewidth is set to be 200 nm and the depth is nearly 300 nm. (b) The solid state etching results on a 250 nm thick evaporated silver film with 10 nm seed Cr layer on top of a glass substrate, showing a complementary nanopattern to that on the stamp. (c) Perspective view of the generated pattern. (d) Close-up view of the alphabet with 200 nm linewidth, showing an aspect ratio better than 1.

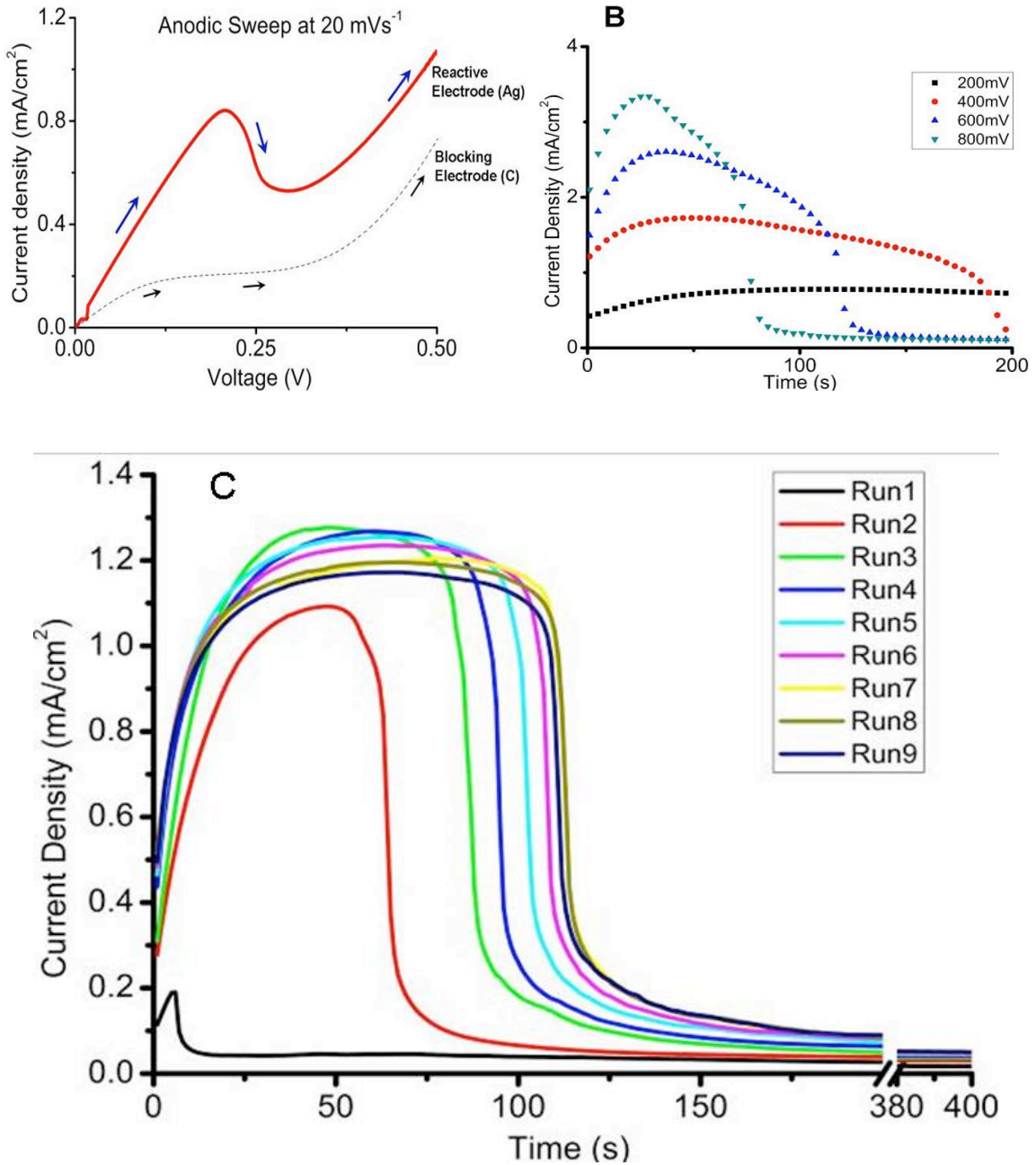


Figure 1.3 (a) Anodic sweeping of a Ag_2S stamp and reactive anode (Ag) or blocking (Carbon) anode obtained at 20 mV/s provides clear evidence of ionic activity between 0.1 and 0.25 V ; (b) The evolution of total current over etch time for the S4 stamping process run at 4 different applied bias with a silver sulfide stamp and silver substrate. The three (0.4 , 0.6 and 0.8 V) that were run to completion show distinct phases of the processes from build up of ionic transport to a steady state followed by a sharp decline as silver gets depleted at the anode; (c) Studies indicate potential of a very repeatable process. The current curves for nine repetitions of a stamping operation with a single new stamp at 0.3 V bias on 80 nm evaporated silver film substrate indicate convergence of the process to a steady-state repeatable current-time profile.

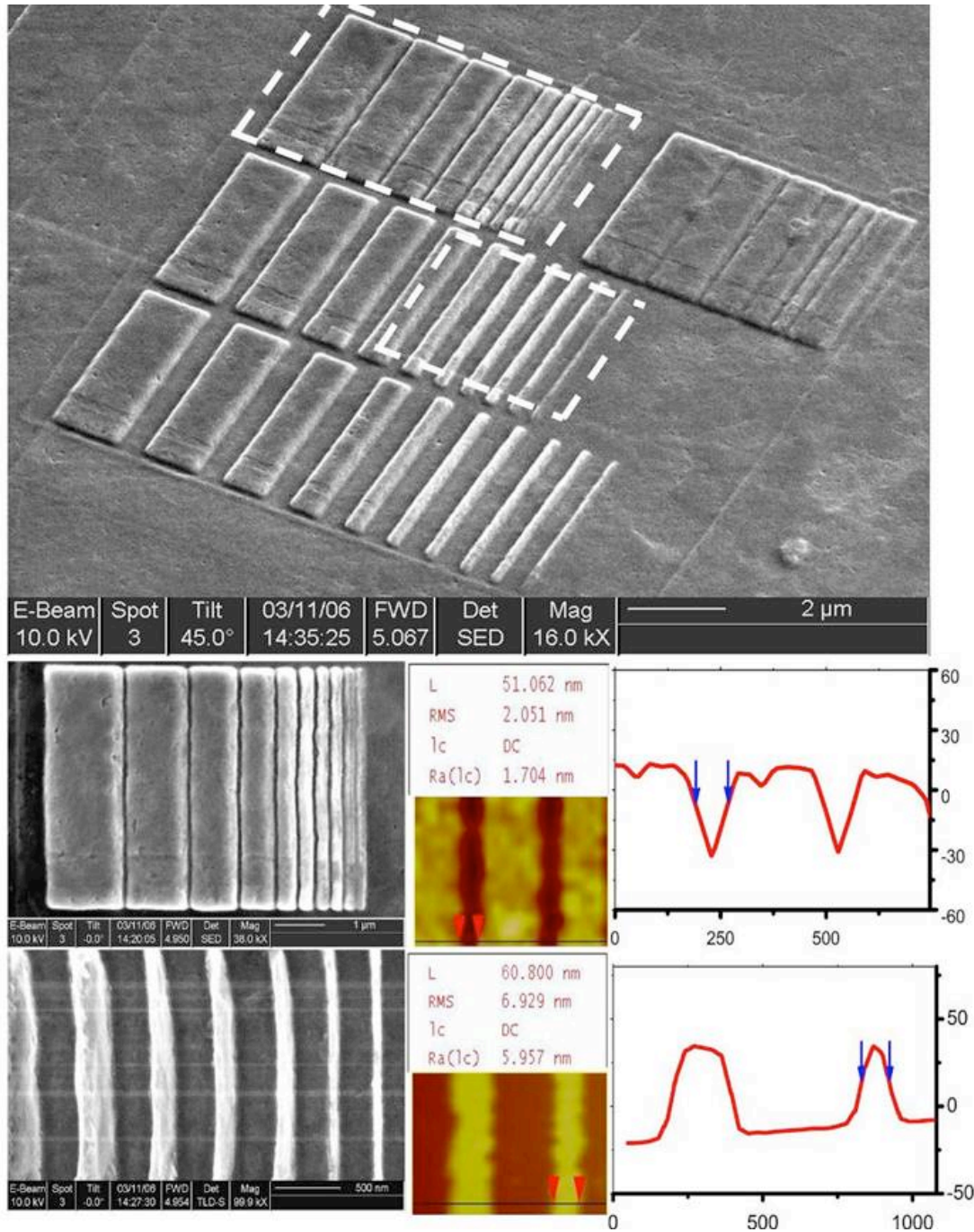


Figure 1.4 Demonstration of high resolution transfer of channels and lines of varied width and spacing. (The line widths for all 4 sets of lines are 1600 nm, 1200 nm, 900 nm, 600 nm, 400 nm, 250 nm, 210 nm, 170 nm, 90 nm and 60 nm from left to right. The spacing is as follows: 50 nm for the line set on the top-left corner, 30 nm for the top-right set of lines by design but did not transfer onto the silver film, 200 nm for the center set, and 350 nm for the bottom set of lines. The feature height is around 100 nm for the thicker lines and reduces to 40 nm for the last two lines of width 90 nm and 60 nm.) Bottom panel: SEM and AFM of the fine trenches and ridges patterned onto silver film. The red curves are cross-sectional profile of the AFM topographic images (bottom middle), showing 50nm trenches are etched with at least 30nm in depth, and 60nm ridges displaying a height of 50nm

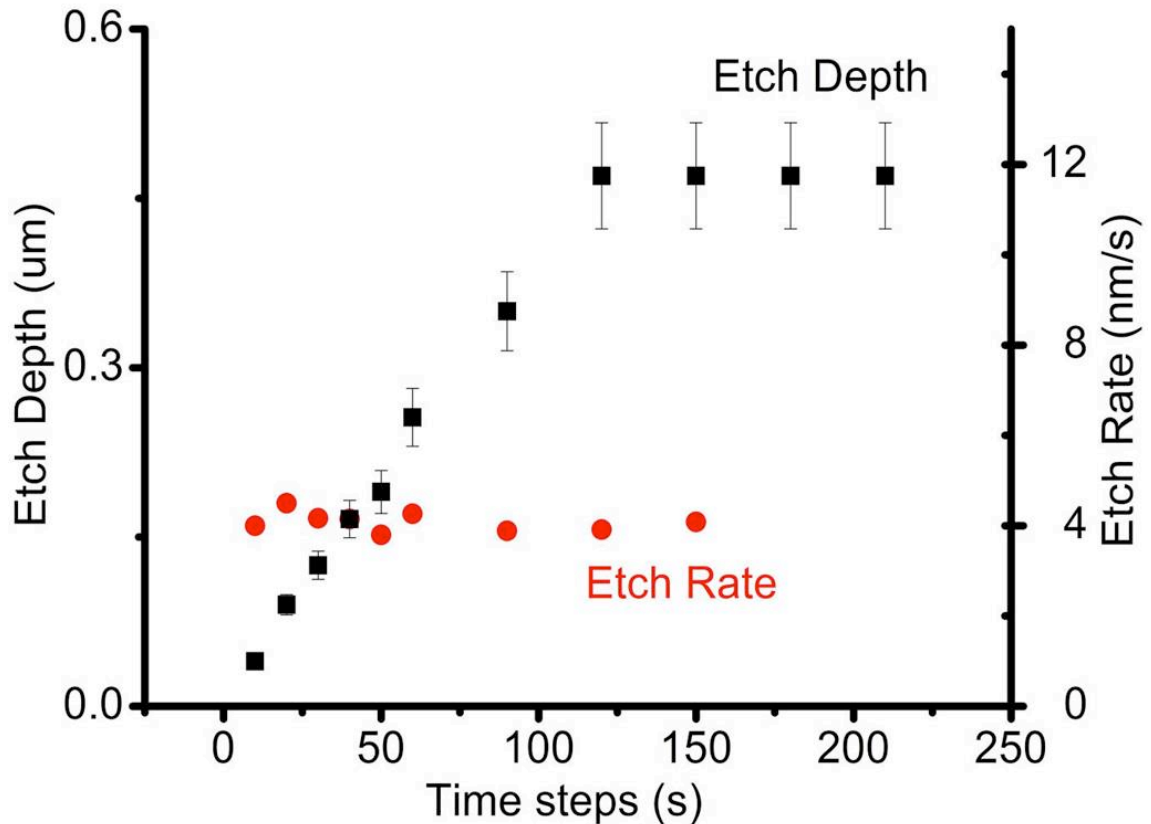


Figure 1.5 Steady state etch rate for fully polarized Ag₂S stamp at applied bias of 0.3 V. The sample is a 470 nm-thick silver film (amorphous silver film on borosilicate glass, samples from Arrandee™). It indicates that, for a constant applied bias, the etch rate remains nearly constant and is independent of the depth to which the stamp has already traveled, facilitating the etching depth control

1.5 REFERENCES

1. M. Madou, Fundamentals of Microfabrication, 2nd Ed., CRC press New York, 2002.
2. W. S. Ruska, Microelectronic Processing, McGraw-Hill, New York, 1987.
3. S. Y. Chou et al., Nanoimprint lithography, J. Vac. Sci. Technol. B, Vol. 14, No. 6, 1996.
4. S. Y. Chou et al., Sub-10nm imprint lithography and applications, J. Vac. Sci. Technol. B 15(6), 1997.
5. S. Zankovych et al., Nanoimprint Lithography: challenges and prospects, Nanotechnology, 12 (2001) 91-95.
6. A. L. Trimmer et al., Single-step electrochemical machining of complex nanostructures with ultrashort voltage pulses, Appl. Phys. Lett., Vol 82, No. 19, 2003.
7. B. Bhattacharyya et al., Electrochemical micro-machining: new possibilities for micro-manufacturing, J. of Materials Processing Technology, Vol. 113, 1-3, 2001, 301-305.

8. H. Rickert, *Electrochemistry of Solids*, Springer-Verlag, 1982.
9. R. Schuster, V. Kirchner, X. H. Xia, A. M. Bittner, G. Ertl, *Nanoscale Electrochemistry*, *Phys. Rev. Lett.* 80, 5599 (1998).
10. P. Avouris, T. Hertel, R. Martel, *Atomic force microscope tip-induced local oxidation of silicon: Kinetics, mechanism, and nanofabrication*, *Appl. Phys. Lett.* 71, 285 (1997).
11. Terabe et al., *Ionic / electronic mixed conductor tip of a scanning tunneling microscope as a metal atom source for nanostructuring*, *Applied physics letters*, Vol. 80, No. 21 2002.
12. Terabe et al., *Formation and disappearance of a nanoscale silver cluster realized by solid electrochemical reaction*, *Journal of applied physics*, Vol. 91, No. 12 2002.
13. F. Prinz, et al, *Electrochemical nanopatterning of Ag on solid-state ionic conductor RbAg₄I₅ using atomic force microscopy*, *App. Phy. Letters*, Vol 85, No. 16, 2004.
14. R. D. Armstrong, T. Dickinson, and P. M. Willis, *The Anodic Dissolution of Silver Into Silver Rubidium Iodide*, *Electroanal. Chem. And Interfac. Electrochem.*, 57(1974)231.
15. M. Hebb, *Electrical conductivity of silver sulfide*, *The journal of chemical physics*, Vol. 20, No. 1, 1952, 185-190.
16. C. Wagner, *Investigations on Silver Sulfide*, *The Journal of chemical physics*, Vol. 21, 1953, 1819-1827
17. *Silver atomic mass: 107.87 g/mol, density: 10.49g/cm³*, W. Callister, *Materials Science and Engineering: An Introduction*, Wiley.
18. R. Hans, *Electrochemistry of Solids*, Springer-Verlag, Berlin Heidelberg New York.,1982, 165-166.

CHAPTER 2.

S4 PROCESS FOR HETEROGENEOUS SYSTEMS: Ag_2S AND COPPER

2.1 INTRODUCTION

Emerging nanotechnology is increasingly focused on the design and manufacture of nanoscale electronic, photonic, mechanical and chemical devices that exploit unique physical and chemical properties [1, 2] and phenomena observed at the nanoscale. Metallic structures play a crucial role in these novel nanodevices and systems as both functional components and as a means for accessing them. However, the common practice for generating metallic patterns has relied on an indirect approach: nanoscale patterns are first created on photoresist by optical lithography or by mechanical imprinting, [3, 4, 5] and followed by metal deposition and subsequent lift-off or etching processes. The damascene process that is widely used by the semiconductor industry, for instance, deposits the copper interconnects electrochemically into the trenches of patterned dielectrics and uses chemical mechanical polishing to remove excess metal in an expensive, complex, multi-step process that requires stringent process environment control and very costly equipment. Other methods such as electrochemical micromachining have been proposed to directly produce sub-micron metallic features.[6, 7] However, significant limitations on lateral resolutions of features produced due to a considerable diffusion length of the reacting species and accelerated etching at sharp edges and corners lead to low geometrical fidelity in the pattern transferred from the electrochemical tool to substrate surface.

Copper is one of the most widely used metallic materials for micro electronics and multi-layer circuit interconnects because of its electrical, mechanical and chemical properties. The need for achieving high process yield and better device performance has called for intense research on the aforementioned nanopatterning techniques for the fabrication of copper features.[1, 2, 3] The multi-step nature of these techniques and the use of mechanical polishers, however, are likely to introduce impurities and residual stress into the resulting copper structure. While the presence of impurities introduces electron scattering sites, the existence of residual stress promotes electromigration of the grain boundaries, both leading to the increase in electrical resistance in the resulting copper structures and are undesirable in implementing copper structures into micro-electronics.[8, 9, 10]

In chapter 1, we demonstrated a solid-state electrochemical imprinting process – Solid State Superionic Stamping (S4) – which directly creates high resolution metallic nanopatterns in a single step.[11-13] At the core of this technique is a solid electrolyte with engraved nanopatterns. During the electrochemical nanoimprint process, highly confined anodic dissolution of metallic nanostructure take place at the stamp-substrate interface, and subsequently, metal ions migrate through the solid electrolyte. For example, with the use of a silver sulfide (Ag_2S) stamp, silver features with resolution smaller than 50nm were achieved with high pattern-transfer fidelity. This approach thus clearly overcomes the limitations of liquid ECM [6,7, 14, 15] where the spatial resolution depends on limited diffusion lengths or confinement of liquid electrolytes. Being a parallel process, the S4 process also offers the potential of high-throughput and excellent etch selectivity. By application of solid electrolyte with high ionic conductivity at room temperature, our preliminary work shows typical etch rates as high as 4 nm/sec, comparable to commercial reactive ion etching processes. This

makes the S4 technology more favorable compared with probe-based direct-writing techniques [16, 17] which draw metallic lines and dots electrochemically from a solid electrolyte, as the latter suffers from limited control in feature dimension and patterning throughput.

Based on the principles of S4 process, in this letter we explore the possibility of patterning metallic nanostructures through the use of a solid ionic conductor stamp which can accommodate different mobile ion species in the host matrix. In particular, we focus on exploiting the conduction channels and defect network in silver sulfide as a host matrix for guest copper-cation incorporation and migration to achieve nanopatterning of copper as conceptually depicted in [Figure 2.1](#). In ambient conditions, silver sulfide is known to have solubility for copper within the range of $0 < x < 0.1$, forming compound $\text{Ag}_{1+x}\text{Cu}_{1-x}\text{S}$. It also displays a mix-ionic conductivity of both Cu and Ag with a ratio of $\sigma_{\text{Ag}}/\sigma_{\text{Cu}}=0.72$. This is a result of both the solubility and the large number of available interstitial sites and conduction channels for cation migration in its open lattice.[18] In addition, the diffusivity of copper ions in Ag_2S matrix, though slower than that of silver ions, reaches as high as $7 \times 10^{-6} \text{cm}^2/\text{s}$ at temperatures below 400C.[19,20] This indicates that, with a small over potential imposed on the interface of Cu with Ag_2S and a potential gradient across the Ag_2S matrix, the dissolution of Cu on this interface can be sustained by the continual diffusion of copper away from the interface, through the Ag_2S matrix and that the solid ionic stamping of Cu can be achieved with Ag_2S as a stamp.

2.2 EXPERIMENTAL

To prepare a silver sulfide stamp, silver sulfide was synthesized and shaped into stamps according to the procedure by Hsu et al [11-13]. The grating pattern on the 300- μm -mesa, as shown in [Figure 2.2\(a\)](#), was produced by direct embossing of the silver sulfide stamp against an SPM calibration grating (model TGX1 from NT-MDT) with 1.59GPa of pressure #.

Copper substrates were prepared by electron beam evaporation onto a 300- μm thick glass cover slip cleaned using RCA1 solution. The copper films were deposited over a 10 nm Cr adhesion layer at a chamber pressure of 3×10^{-6} torr and a stable rate of 0.1nm/s.

Cu nanopatterning through Cu percolation was performed in ambient environment at room temperature. Nanopatterning started by bringing the pre-patterned surface of a silver sulfide stamp into contact with a copper substrate with controlled pressure of 1GPa. Dissolution of Cu on the copper-silver sulfide interface was initiated by applying a potentiostatic voltage of 0.4V across the interface controlled by a digital potentiostat (Gamry Instrument model Reference 600), and proceeded through the thickness of the copper film, 40nm. The patterned copper substrate was then examined by AFM, running at tapping mode using an ultra-sharp tip with a resonant frequency 485kHz. The results are shown in [Figure 2.2](#). Shown in the bottom panels are SEM images of a Cu meander wire made by the same procedure, confirming the lateral resolution achieved is 60nm for line width and the capability to produce high aspect ratio pattern.

To characterization of the copper-silver sulfide interfacial electrochemical activity, a set of experiments of electrochemical impedance spectroscopy was performed between the silver sulfide stamp and a 40 nm thick copper substrate (the anode) with an 20mV AC and scan frequencies from 10mHz to 1MHz (Figure 3A and 3B). An equivalent circuit model (figure3C) was also proposed for the interface reaction and transport of Cu.

2.3 RESULTS AND DISCUSSION

To validate the proposed concept of copper nanopatterning with percolation of Cu through Ag₂S, square patterns on the stamp, such as those shown in [Figure 2.2\(a\)](#), were produced by directly embossing the patterns into silver sulfide stamps using a silicon calibration grating (model TGX1 from NT-MDT) and then performing the S4 stamping process on a copper film with the silver sulfide stamp. The feature depth on the stamp in [Figure 2.2\(a\)](#) was about 600nm while the copper film being patterned was 50nm in thickness, ensuring enough pattern-relief depth. As shown in [Figure 2.2\(b\)](#) the copper film was patterned, demonstrating, for the first time, the S4 technique with an Ag₂S stamp that exploits the inter-diffusion phenomenon of Cu ion in Ag₂S lattice. As further investigation on the copper-patterning resolution of this new approach, a meander line of 60nm in line-width and 650um in length was carved into a silver sulfide stamp. A copper wire of 50nm in width and 650um in length was created using the Ag₂S stamp and the S4 process, demonstrating the high-resolution capability of this new approach proposed in this letter.

To further study the interface phenomena of the Cu-Ag₂S system, i.e. the Cu dissolution on the substrate, the incorporation of such ions into the Ag₂S matrix, as well as the migration of those ions through the space charge region adjacent and into the bulk region, electro-impedance spectroscopy, EIS, was carried out. As seen in [Figure 2.3a](#), the frequency response of the system basically transitions from high impedance with small phase shift in the low frequency regime to low impedance but large phase shift in the higher frequency domain (> 10 kHz). From the Nyquist plot shown in figure 3b, it can be clearly seen that the system has two distinct regions with different impedance response to input frequency. As observed in the work of Armstrong,[21] in the case of superionic conductors, the anodic dissolution rate and hence the flow of metal into solid electrolyte is governed by several mechanisms including direct charge transfer, surface adatom diffusion, as well as the growth and nucleation of 2-dimension pores on the metal surface with each being the rate limiting mechanism at different anodic surface overpotential ranges. The understanding of these processes is crucial to refining the process parameters of the S4 on Cu with Ag₂S in order to optimize process yield and obtain highest-possible patterning rate. At the voltage level used in our spectroscopy measurements, the frequency response is very likely the result of two competing mechanisms: the Cu atatom diffusion from surface pore nucleation sites to the metal-electrolyte-pores tri-phase contact points, and the subsequent charge transfer process resulting from the copper oxidation.[20] The advantage of using EIS to examine interface phenomenon is that physical constants and properties of the metal-electrolyte system can be determined through the use of an equivalent circuit to model the measured impedance spectroscopy results. As summarized by Maier,[22] the connections between the elements used in

an equivalent circuit to model such a system and the actual physical properties of the system can be expressed as:

$$R_j^{int} = \frac{k_B T}{e^2 z^2 c_{eq} A} \dots \text{Equation 2-1}$$

$$C_j^{int} = \chi \chi_0 \frac{A}{L_{Dj}}, \text{ where } L_{Dj} = \sqrt{\frac{\chi \chi_0 k_B T}{e^2 z^2 c_{eq}}} \dots \text{Equation 2-2}$$

$$W_j = \frac{B}{\sqrt{\omega}} \quad (1) \quad , \text{ with } B = \frac{k_B T}{z F A C D \sqrt{C D}} \frac{11}{\sqrt{\frac{\chi \chi_0 k_B T}{e^2 z^2 c_{eq}}}} \dots \text{Equation 2-3}$$

2-3

$$C_{geo} = \chi \chi_0 \frac{A}{L} \dots \text{Equation 2-4}$$

where k_B =Boltzmann constant, T =temperature, e =electron charge, z = charge number, c_{eq} = equilibrium concentration, k =reaction constant, A =area, $\epsilon \epsilon_0$ =dielectric constant, L_D = double layer thickness, ω =excitation frequency, F =Faraday's constant, D =diffusion coefficient. R_{int} and C_{int} are the interface resistance and capacitance resulting from dissolution reaction, W is known as the Warburg impedance existing in systems where the influence of ionic diffusion plays a role in interface reaction, C_{geo} is geometric capacitance resulting from the dielectric properties of the solid electrolyte and system geometry.

The proposed equivalent circuit model is based on the following physical picture: on the solid interface the copper dissolution starts with the formation and surface migration of copper adatoms towards the actual contact between the solid copper phase and the solid electrolyte. As these adatoms reach these tri-phase points they

then proceed to oxidation to form copper ions and free electrons. The resulting copper ions are incorporated into the silver sulfide lattice and start their migration through in space charge region and then across the bulk solid electrolyte. This process is modeled as a resistor for the adatom migration in series with the parallel combination of an interface resistor and the series combination of a Warburg impedance and a capacitor for the oxidation reaction and then in series with another resistor for the migration of copper ions in the silver sulfide. This circuit is then placed in parallel connection with another circuit (which is similar but without the diffusion effects) that models the electronic part of the conduction because of the mixed conduction nature of silver sulfide, and a geometrical capacitor.

The results of the experiment data fitting shown in [Figures 3.3a](#) and 3.3b with this model gives an interface capacitance of $4.9\mu\text{F} \pm 0.5\mu\text{F}$ and an interface resistance of $5.3\text{M}\Omega \pm 0.6\text{M}\Omega$, giving rise to a time constant of around 26s at a potential level of 20mV. This time constant is strongly related to the screening length L_{Dj} as seen in equation 2 where it is inversely proportional to the interface capacitance C_{int} . As shown in Armstrong's work the interface capacitance decreases as the anodic overpotential increases [21], it is thought that the time constant estimated with our proposed equivalent circuit would decrease as the anodic overpotential increases. In fact, in our electrochemical stamping experiments where the applied anodic potential was 0.4V, a time constant of around 1s was observed, indicating a much smaller interface capacitance and longer screening length stretched by the increased potential gradient in the bulk solid electrolyte. Through manipulation of the above equations a screening length of about 20nm is obtained, which falls in the range of typical screening lengths seen in solid-solid electrolyte systems [21]. Further, using equation 2-2, a surface equilibrium copper adatom/cupric ion concentration on the order of 10^{12}

$/\text{cm}^2$ is estimated, suggesting only 0.1% of surface atoms are in the adatom state [22]. In light of the sparsity of the adatom and the dependency of its diffusion rate on temperature, this also suggests that the copper adatom formation and diffusion are the rate limiting steps of the dissolution process on the interface under our experimental conditions, agreeing with our predictions earlier. A further estimation from equation 2-1 suggests a copper adatom oxidation rate k_f on the order of 10^{-10} m/s at the excitation potential of 20mV. With this estimation of the oxidation rate along with the surface concentration and the Chang-Jaffe boundary condition [23], an exchange current density only on the order of $10\text{nA}/\text{cm}^2$ is also estimated. This estimation, although quite low when compared to typical liquid-state electrochemical reactions involving copper, is reasonable considering the dependence of reaction rate on copper adatom concentration(reactant), temperature(room temperature), and the nature of contact at a solid-solid electrolyte interface. In understanding these physical properties and how the dissolution process revolves around these properties, we are working to use controllable process parameters such as pulsed-voltage supply, contact pressure, etc. to introduce perturbations on the effects of these physical properties on the S4 process yield. At the same time, through the understanding of the interactions of the two materials on the interface, a knowledge base can be built for interdiffusion-based self-assembly of nanowires and nanostructures. Further, novel applications such as localized altering of material composition in nanometer domains can be explored.

2.4 CONCLUSION

In summary, we presented in this paper a simple and parallel approach to directly patterning copper nanostructures with substitutive electrochemical reactions in solid

state. The process works under ambient environmental conditions and does not require complex process steps or expensive equipment. The process can easily be scaled up for high-throughput production, as it can operate at room temperature, and only requires low voltages and nominal pressure. Furthermore, fabrication of the stamp is simple as relief patterns can be created in Ag₂S by simply embossing with a master (for example, a silicon master made by conventional lithography techniques). This technique will enable the direct patterning of metallic nanostructures in fabricating chemical sensors, photonic and plasmonic structures, and electronic interconnects.

2.5 FIGURES

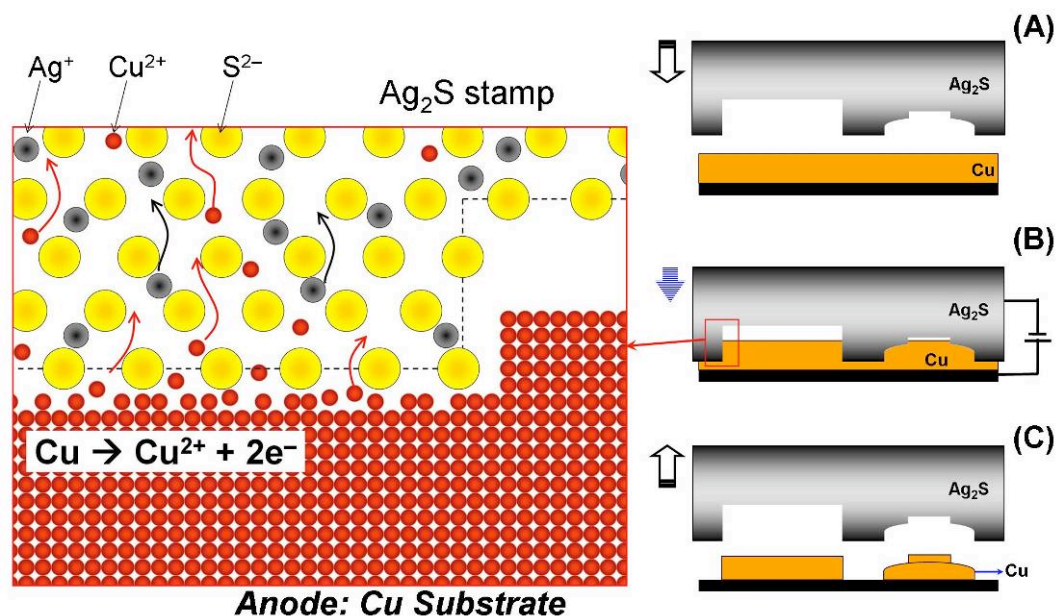


Figure 2.1 Schematics depicting the Concept of metal nanopatterning with S4 in heterogeneous systems. A stamp made of a solid electrolyte is brought into contact with the workpiece or substrate to be patterned. A biased anodic surface overpotential dissolves the metal at the anode-stamp interface. (A) To initiate solid state ionic stamping, a pre-patterned solid electrolyte (silver sulfide in our work) backed with an inert metal is connected to a potentiostat as the counter electrode (cathode) and the metal substrate to be patterned is the anode. (B) The pre-patterned solid electrolyte stamp is brought into contact with the metal workpiece or substrate and, with an applied voltage bias and nominal contact pressure, electrochemical etching takes place at the contact areas progressively, dissolving metal into the solid ionic stamp and engraving the workpiece. (C) Electrochemical nanoimprinting is completed, resulting in a pattern on the metal substrate complementary to that on the solid electrolyte stamp

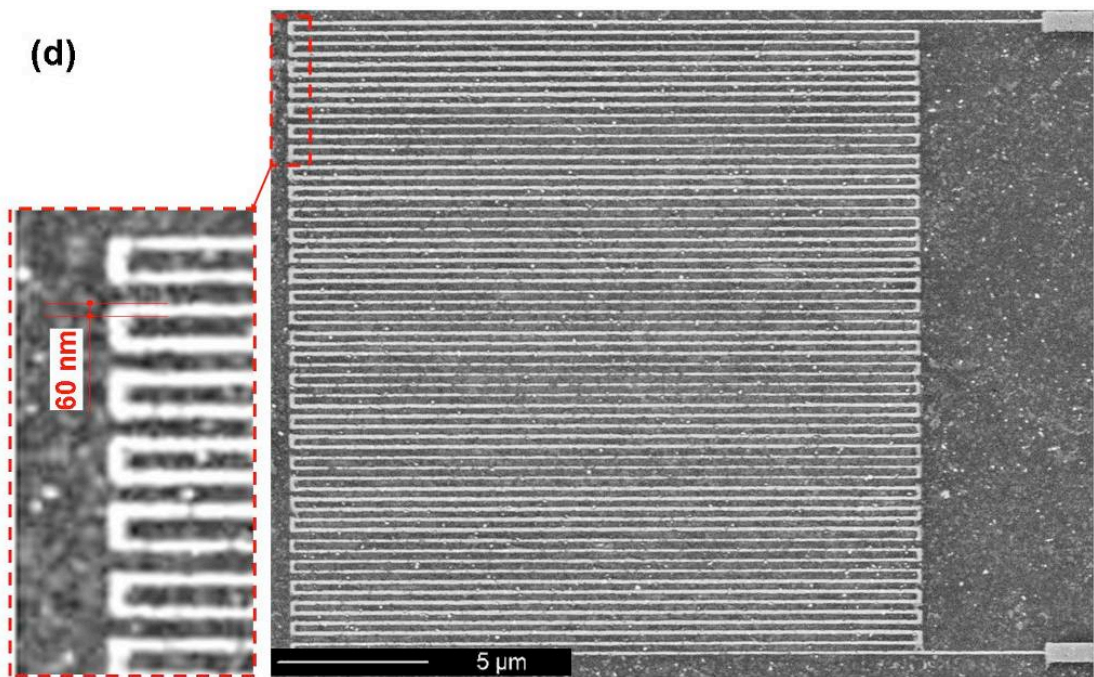
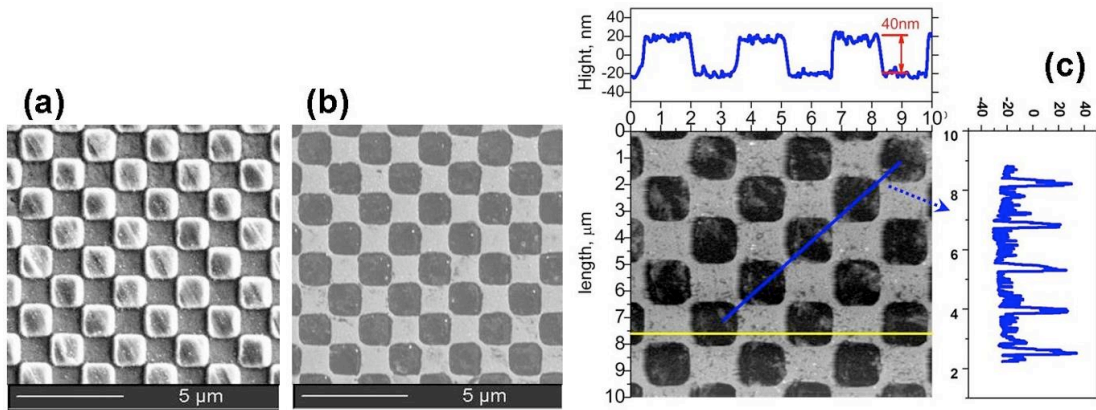


Figure 2.2 (a) and (b) are SEM images of the square pattern of Ag_2S stamp made by embossing into a silicon mold and the resulting Cu pattern generated by the S4 process with Ag_2S . The raised squares are $1.6\mu\text{m} \times 1.6\mu\text{m}$, and the spacing between them $1.4\mu\text{m} \times 1.4\mu\text{m}$. The depth of the squares is around 600nm , the copper features generated are of the high dimension transfer fidelity (c) AFM images showing the lateral dimension of the copper pattern. (d) Cu meander wires of 60nm in line width and $650\mu\text{m}$ in length.

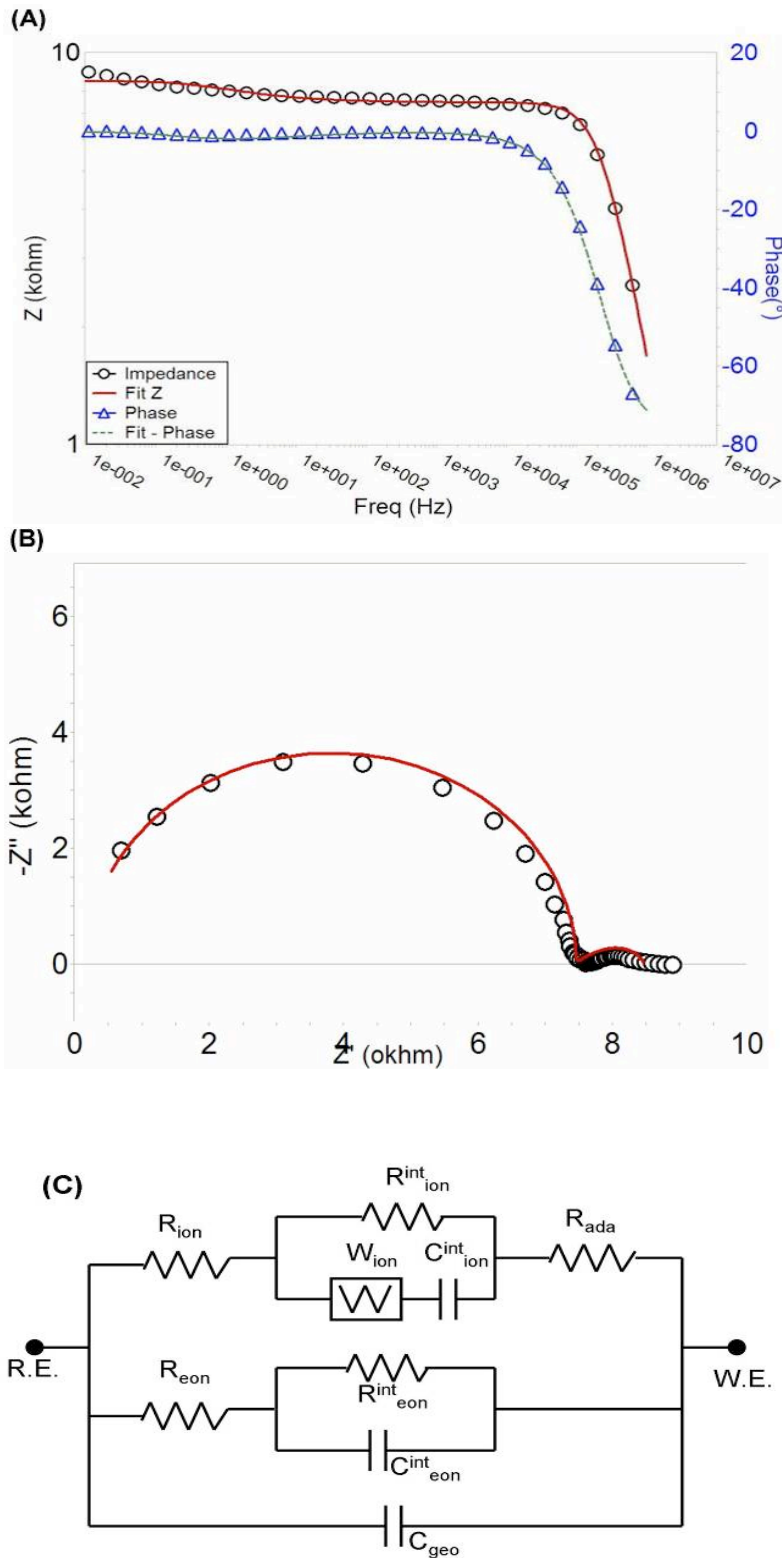


Figure 2.3 Electro-impedance spectroscopy measurement of Cu/Ag₂S/C. (a) Bode plot and (b) Nyquist plot of the impedance measurement, from which the interfacial capacitance ($C=4.9\mu\text{F}$) and resistance ($R=5.3\text{M}\Omega$) are fitted, giving rise to a time constant $t=26\text{s}$ required for Cu ion transfer through the interface. (c) Proposed equivalent circuit for the interface reaction and transport of Cu.

2.6 REFERENCES

1. M. Madou, *Fundamentals of Microfabrication*, 2nd Ed., CRC press New York, 2002.
2. W. S. Ruska, *Microelectronic Processing*, McGraw-Hill, New York, 1987.
3. S. Y. Chou et al., Nanoimprint lithography, *J. Vac. Sci. Technol. B*, Vol. 14, No. 6, 1996.
4. S. Y. Chou et al., Sub-10nm imprint lithography and applications, *J. Vac. Sci. Technol. B* 15(6), 1997.
5. S. Zankovych et al., Nanoimprint Lithography: challenges and prospects, *Nanotechnology*, 12 (2001) 91-95.
6. A. L. Trimmer et al., Single-step electrochemical machining of complex nanostructures with ultrashort voltage pulses, *Applied Physics Letters*, Vol 82, No. 19, 2003.
7. B. Bhattacharyya et al., Electrochemical micro-machining: new possibilities for micro-manufacturing, *J. of Materials Processing Technology*, Vol. 113, 1-3, 2001, 301-305
8. M. Hampden-Smith, New routes to Cu-patterned Teflon substrates, *Advanced Materials*, 1992. 4, No 7/8
9. R. Gonella et al., Process steps impact on electrical and electromigration performances of dual damascene copper, *2000 IRW final report*, IEEE
10. W. Stainhogl et al., Comprehensive study of the resistivity of copper wires with lateral dimensions of 100 nm and smaller, *Journal of Applied Physics*, 97, 023706 (2005).
11. K. Hsu, N. Fang, P. M. Ferreira, Pattern Transfer by Solid State Electrochemical Stamping, *US patent application # 11/376,908*, 2006
12. K. Hsu, P. Schultz, N. Fang, P. M. Ferreira, Electrochemical Nanoimprinting with Solid-State Super-Ionic Stamps, *Nano Letters*, *nl062766o*, 2006
13. P. Schultz, K. Hsu, N. Fang, and P. Ferreira, *Journal of Vacuum Science & Technology B: Microelectronics and Nanometer Structures -- November 2007 -- Volume 25, Issue 6*, pp. 2419-2424
14. P. Avouris, T. Hertel, R. Martel, Atomic force microscope tip-induced local oxidation of silicon: Kinetics, mechanism, and nanofabrication, *Applied. Physics. Letters*, 71, 285 (1997).
15. Terabe et al., Ionic / electronic mixed conductor tip of a scanning tunneling microscope as a metal atom source for nanostructuring, *Applied Physics Letters*, Vol. 80, No. 21 2002.
16. Terabe et al., Formation and disappearance of a nanoscale silver cluster realized by solid electrochemical reaction, *Journal of Applied Physics*, Vol. 91, No. 12 2002.
17. F. Prinz, et al, Electrochemical nanopatterning of Ag on solid-state ionic conductor RbAg4I5 using atomic force microscopy, *Applied Physics Letters*, Vol 85, No. 16, 2004.
18. M. Rohnke et al., The influence of non-equilibrium defects on the anodic dissolution of a metal into a solid electrolyte, *Solid State Ionics*, 177, 2006, 447-456
19. R. Kadrgulov et al., Phase relation, ionic transport and diffusion in the alloys of Cu₂S-Ag₂S mixed conductors, *Ionics*, 7, 2001, 156-160
20. N. Krestovnikov et al., *Izvestiya Akademii Nauk SSSR, Neorganicheskie Materialy* (1968),4(7)
21. R. D. Armstrong et al., The anodic dissolution of silver into silver rubidium iodide, *Electroanalytical Chemistry and Interfacial Electrochemistry*, 57 (1974) 231-240.
22. T. A. Nissila et al., Collective and single particle diffusion on surfaces, *Advances in Physics*, 2002, Vol. 51, No. 3, 949-1078.
23. H. C. Chang et al., Polarization in Electrolytic Solutions. Part I. Theory, *Journal of Chemical Physics*, 1952, Vol. 20, Issue 7, pp1071-1077.

CHAPTER 3.

NUMERICAL MODELING OF MIXED ELECTRONIC/IONIC CONDUCTION IN Ag_2S

As mentioned in introduction, the two phenomena that sustain the solid state electrochemical patterning process are the dissolution of solid metal on a metal-solid electrolyte interface and the subsequent transport of the product species away from the interface. While the kinetics and transport of such solid-solid electrolyte pair can differ among different systems, for example the type of metal and the type of conductors considered, for the purpose of discussions pertain to the this work, the metal specie will be limited to silver and the solid electrolyte will be limited to silver sulfide. In this chapter the general formulism for a mixed ionic-electronic system will be first described. This system will be applied and simplified according to the conditions unique to the silver-silver sulfide case. A finite element model based on this transport equation system will be constructed to study the transport of ionic specie in the silver sulfide stamp. Predictions from the numerical model will be discussed and compared to experimental results. As last, this model will be extended to combine with silver-silver sulfide interface kinetics to solve for the current evolution observed from experiments

3.1 INTRODUCTION TO MIXED ELECTRONIC/IONIC CONDUCTION IN SILVER SULFIDE, Ag_2S

As one of the supporting mechanism for the solid-state electrochemical patterning process, the transport of product silver ions away from the interface is the key to the progression of this process. Silver ions, however, are not the only mobile specie in silver sulfide. In silver sulfide both electrons and ions can carry charge. It is also recognized to possess the electrical properties of an n-type semiconductor with an electronic conduction band gap of $\sim 1.3\text{eV}$.

The decoupling of such mixed conduction into its electronic and ionic component has historically been carried out by setting up the respective Nernst-Planck equations of the electronic and ionic species. Such equation sets are usually of the form

$$j_e = \sigma_e \nabla \left(\frac{\mu_e}{e} - \phi \right), \text{ and}$$

$$j_i = -\sigma_i \nabla \left(\frac{\mu_i}{e} + \phi \right),$$

Where j_e is the electronic current density and j_i the ionic current density, μ_e and μ_i are the chemical potentials of electrons and ions in silver sulfide. ϕ is the electrical potential experienced by the species.

These equations are setup under the relations between chemical potentials and electrochemical potentials only pertain to the silver sulfide compound. Under special end conditions such as fully-blocking and fully-reversible conditions for either electronic or

ionic species, these equations can be solved analytically. In fully-blocking boundary conditions, either the ionic or electronic specie is blocked from passing through an interface.[1-5] However, none of the these conditions are present in our stamping process and a set of equations and coupling boundary conditions need to be developed.

As introduced in chapter 1, in the solid state electrochemical stamping process, when the solid electrolyte is brought into contact with the metal electrode to be patterned, an anodic dissolution reaction takes place in the metal-solid electrolyte interface upon raising the electrical potential of the electrode. The dissolved metal ions have to be carried away from the interface region in order for the dissolution to continue take place. As such, the coupled ionic-electronic transport in the solid electrolyte needs to be considered in conjunction with the reaction kinetics on the metal-solid electrolyte interface. The formulation for such transport is similar to that for liquid-state ionic transport in solutions. The flux of a charged specie in an electrochemical environment is proportional to the gradient of electrochemical potential this species experiences. The proportional constant is defined as the conductivity of such species.

$$j_{kkk} = \sigma_k \nabla \tilde{\mu}_k \quad \dots\dots \text{Equation 3-1}$$

where k = ion or electron, σ is the conductivity, $\tilde{\mu}_k$ is the electrochemical potential of the specie. The electrochemical potential can be written as the sum of the chemical potential and the electrical potential experienced by the species of interest.

$$j_k = \sigma_k \nabla (\mu_k + z_k FV) \quad \dots\dots \text{Equation 3-2}$$

where μ and V are the chemical potential. When combined with mass conservation of

species, the transient response of transport of a charged species in the presence of an electrochemical field can be expressed as

$$\frac{\partial c_k}{\partial t} = \nabla \left\{ -D_k \nabla c_k + \mu_k F c_k \nabla V \right\} \dots \text{Equation 3-3}$$

In typical transport problems in electrochemical systems the equations set is coupled with charge neutrality (which states that the total charge change is zero) and solved numerically with appropriate end conditions. In the case of the transport of product silver in the silver sulfide stamp in the solid-state electrochemical patterning system, charge neutrality conditions are violated because of the experimental conditions. In the experiments, the metal electrode is in chronoamperometry mode wherein the electrical potential of the metal electrode is controlled by a potentiostat to be a constant value relative to a reference electrode attached to the electrolyte and the current flowing through the system is measured. As such, the electric potential between the metal electrode and the back electrode of the solid electrolyte stamp is maintained by removing the electrons generated by the dissolution reaction of the metal electrode from the system. The result of this is that the number of metal ions in the solid electrolyte increases during stamping (product ions from the reaction of the metal electrode-solid electrolyte interface) while the number of electrons in the system remains more or less constant. Therefore charge neutrality between electron and silver ion in the silver sulfide domain is violated.

In addition to the violation of charge neutrality, the conductivity of electrons is higher than that of silver ion in silver sulfide by about 3 orders of magnitude. This situation is

realistically similar to that of an electrophoretic cell with a supporting electrolyte whose conductivity is much larger than that of the specie considered. In such conditions, the charge transport is mainly carried by the supporting electrolyte and the transport of the specie considered is mainly diffusive but with some migrative flow due to the finite conductivity of the supporting electrolyte. The transport of silver ions from silver dissolution in silver sulfide is similar to this picture. Most of the charge transport is carried by the electrons that are flowing in the system, and the transport product silver ions is mainly diffusive but with some migrative contribution due to the finite conductance of electrons. This electrophoretic process can be modeled by setting up a Nernst-Planck equation for the ionic species and a DC conduction one for the electronic species. The two equations are then coupled by the relation unique to silver sulfide which describes the changes in the electronic conductivity of electrons when the chemical potential (or equivalently the concentration) of silver in silver sulfide.

$$\frac{\partial c_{Ag}}{\partial t} = \nabla \left\{ -D_{Ag} \nabla c_{Ag} + \mu_{Ag} F c_{Ag} \nabla V \right\} \dots \dots \text{Equation 3-4}$$

$$-\nabla \left(\sigma_e \nabla V - J^{ext} \right) = 0 \dots \dots \text{Equation 3-5}$$

$$\text{and } \sigma_e = \sigma_e^0 \left(1 + \frac{c_{Ag}}{c_{Ag}^0} \right) \dots \dots \text{Equation 3-6}$$

where c_{Ag} , c_{Ag}^0 , D_{Ag} , μ_{Ag} are the concentration, intrinsic concentration, diffusivity, and mobility of silver in silver sulfide respectively. σ_e is the electronic conductivity of silver sulfide, F is Faraday's constant, and V the applied voltage to the system.

A Finite Element model is setup based on these equations in commercial software COMSOL to solve for the transport of silver ions in silver sulfide during a stamping process.

3.2 MODEL SETUP, PROPERTIES, AND END CONDITIONS

As seen in [Figure 3-1](#) the 2D model is setup such that the geometry of the electrolyte domain and electrode configuration is the same as experimental conditions. The small mesa at the bottom represents the metal substrate-solid electrolyte contact during stamping and the backing electrodes are in contact with the silver sulfide on the sides as in experiments the silver sulfide stamps are held by a machined stamp holder and the actual contact is on the sides of the stamp.

The material properties as well as the source of the data acquired are tabulated in [Table 3-1](#). The intrinsic charge carrier number is used as the initial condition for concentration. Einstein's relation is used to evaluate the mobility of silver in silver sulfide.

The silver ion influx boundary condition is set such that it resembles the actual conditions in stamping experiments. As shown in chapter two, the etch rate ramps up quickly to a steady value and remains constant throughout the thickness of the silver film being etched. It then drops to zero when the film is depleted. The values of etch rate, R_{et} , are obtained from experimental measurements of etch rate at a particular applied potential, as shown in [Figure 1-5](#).

The ionic conductivity in silver sulfide is known to have originated from its ability to

deviate from its perfect stoichiometry: from $\text{Ag}_{1.998}\text{S}$ to $\text{Ag}_{2.002}\text{S}$. This implies that the charge carrier concentration of a silver sulfide stamp of perfect stoichiometry will have 0.1% of the total silver in silver sulfide becoming available for carrying ionic current. The intrinsic ion concentration here is obtained by first calculating the amount of silver (87.06% of molar mass of Ag_2S) in silver sulfide (molar mass 247.8 g/mole) followed by calculating the mole volume of this silver amount with the density of silver sulfide (7.234g/cm^3). The inverse of the molar volume gives the total amount of silver in silver sulfide; and 0.1% of this amount is then the intrinsic charge carrier concentration in silver sulfide.

3.3 SIMULATION RESULTS AND DISCUSSION

Figure 3-2 shows the numerical results for conditions stated in the previous section. Three quantities are presented in each plot: the instantaneous spatial distribution of the stoichiometry of silver sulfide stamp (color map), electrophoretic flux of silver species (arrows), and electrical potential distribution (contour lines). All three quantities are presented at four temporal points of importance- 0 second, 95 seconds (during metal etching), 105 seconds (right after metal has been depleted), and 300 seconds when the process is terminated. As evident in the results, the electrode configuration induces a distortion of the electrical potential distribution and caused uneven distribution of cathodic reaction, and silver transport and accumulation is mainly toward the leading edge of the electrode on the sides. As a direct result of this, one can observe that the stoichiometry at 300 seconds a small region of the silver sulfide domain close to the

leading edge goes out of the range allowed in silver sulfide, $\text{Ag}_{2.002}\text{S}$. The implication of this is that precipitation of silver from silver sulfide can happen, which will give rise to phase separation and cause electrochemical damages to the stamp. Also can be observed is the change in electric field distribution as the concentration changes. This is a direct result of the coupling between the electronic conduction and the chemical potential of silver as discussed in the section 1.

Shown in [Figure 3-3](#) are the total flux and its migrative and diffusive components at a point 100 μm away from the Ag-Ag₂S interface. One can observe that during the etching portion of this 300sec-patterning process, both migrative and diffusive transport are carrying ions away from the interface with the migrative term being about an order larger. This behavior is the result of an influx of Ag on the interface from the etching reaction, and can only be seen under such conditions. Otherwise the concentration build-up will retard the migrative flux. The short delay in flux increase in the diffusive transport is due to the fact that the point is not right on the interface, and some time is required for the diffusion front to reach this point. At 100 seconds when the influx of silver on the interface is turned off, which represents the depletion of Ag in the actual solid-state electrochemical patterning, one can observe the total flux experience a sharp decrease. The reason is two-fold: the decrease in diffusive flux as well as in migrative flux. As the influx of silver ion on the interface is removed, the concentration gradient buildup due to transport prior to this point (a.k.a polarization effect) very quickly drives the diffusion of silver ions in the reverse direction as indicated in the negative diffusive flux here. While the decrease in diffusive flux is straight forward, the reduction in the migrative flux is due to characteristics unique to Ag₂S and is less intuitive. As discussed

earlier, the increase in chemical potential of silver, or silver concentration, can give rise to an increase in the electronic conductivity of silver sulfide. As such, as the concentration of silver at the point where the flux values are evaluated increase due to the back diffusive flow of silver ions, the increase in local electronic conductivity introduced a shunt effect on the migrative flux of silver. This unique coupling nature of the two charge carrier species in Ag_2S is captured here. The total flux will drop to a steady-state value zero when the chemical potential in the stamp balances out the electrical one.

The stoichiometry of the stamp, as indicated in [Figure 3-2](#), remains un-perturbed during a stamping process except for in the vicinity of the backing electrodes and the metal-electrolyte interface. This is important in terms of life of a stamp in that the electrochemical damages, e.g. precipitation of silver phase and decomposition of silver sulfide, can be avoided. In the two regions where the stoichiometry is affected the most, one can expect changes going beyond the range of $\text{Ag}_{1.998}\text{S}$ to $\text{Ag}_{2.002}\text{S}$. As indicated shown in [Figure 3-4](#), the temporal profile of local stoichiometry at Ag- Ag_2S interface and at the backing electrode- Ag_2S are plotted. One can observe the changes on the Ag- Ag_2S interface has little effect on the stoichiometry at the backing electrode side, the increase in stoichiometry is more or less due to the transport of silver from the domain into the vicinity of the backing electrode region. The stoichiometry of at the Ag- Ag_2S interface region, though, follows a similar trend in changes in local flux. This is not surprising wither since the flux of silver has direct effect on local concentration and stoichiometry.

Although the aforementioned stoichiometry change on the Ag- Ag_2S can follow the changes in local fluxes quite closely, the value has not gone beyond the stoichiometry range of silver sulfide. As discussed in the previously, this implies that this 300second-

patterning process does not introduce electrochemical damages to the silver sulfide stamp in the Ag-Ag₂S interface region. On the other hand, the stoichiometry on the backing electrode side reached its limit Ag_{2.002}S at around 60 seconds into the patterning process. By the end of the process, the stoichiometry in a small region around the edge of the backing electrode has gone beyond the limit, as shown in the white region in the lower right panel in [Figure 3-2](#). This implies that the silver precipitation can happen in this region, causing phase separation. One can avoid this by introducing a larger backing electrode which can even out the silver ion accumulation and can prevent the degradation of silver sulfide. In [Figure 3-5](#) where the stoichiometry across the line between the center and stamp and the backing electrode, one can observe that the stoichiometry change on the Ag-Ag₂S side is mainly within 500um range and at the end of the 300 second-stamping it is still within stoichiometry range of silver sulfide, suggesting no decomposition of silver on the interface. On the backing electrode side, however, the affected region although is smaller, the stoichiometry reached more Ag_{2.003}S, suggesting the possibility of silver precipitation.

It is generally recognized that the transport properties of ionic systems experiences increase when the dimensions of the domain wherein the transport takes place are small as compared to dimensions of the space charge layers or the characteristic length of the diffusive transport. Here in the constructed model features of lateral dimensions ranging from 10nm up to 100nm were investigated. It is found that the with a constant potential and ion concentration imposed on the end of these nano features (which represents the interface of a solid electrolyte stamp and a metallic substrate), the potential gradient as well as the concentration gradient existed in those features increases as the lateral

dimension of the features goes down as can be seen in [Figure 3-6](#). From the result, it is clearly seen that the transport along the length of those features, also increases as the lateral dimension of the feature goes down. The increase in migrative flux is almost two fold when the width of the feature shrinks from 100nm to 10nm. Similar trend is also observed in the diffusive flux. The prediction here suggests that in terms of patterning efficiency, smaller features are preferable for the S4 process in that (as will be discussed in the next section), the silver dissolution rate at the metal-solid electrolyte interface is balanced by the transport properties of silver ions in the solid electrolyte domain, the faster the ions produced from the reaction can be carried away by migration or diffusion, the higher the rate of dissolution can reach under the same driving electrical potential. The model constructed here can also be used to design and evaluate the efficiency of batteries with nano-patterned electrodes.

3.4 SILVER-SILVER SULFIDE INTERFACE KINETICS

In chapter one the dissolution process on the Ag-Ag₂S interface was briefly discussed to illustrate the concept of patterning metal with solid-state electrochemical dissolution. Here more detailed discussion on the dissolution process on the Ag-Ag₂S interface will be discussed. When two solid surfaces are brought into contact, the actual contact between the two surfaces depends very much on the topography of the two, and is usually different from the apparent contact area. Here the actual contact area is, on the scale of the roughness of the surfaces, the points on the asperities of the two surfaces that are in actual contact, and the apparent contact area is the overall size of the surfaces of concern.

Often times, the actual contact area is much less than apparent contact area. In the case of the solid-state electrochemical patterning, the Ag-Ag₂S interface is not exempted from this nature. As seen in [Figure 3-6](#), the simple “dissolution” of silver can consist five processes. These processes are not necessarily in series but can happen simultaneously: adatom formation with a rate constant k₁, surface diffusion of surface adatoms of rate k₂, oxidation of adatoms at the actual contact area with a reaction rate constant k₃, the incorporation of resulting ions across the lattice boundary into the silver sulfide lattice with a rate k₄, and finally the transport of these ions away from the interface of a rate k₅. The formation of adatoms from the defects of the metallic substrate provides abundance of surface adatoms that are mobile on the metal surface. When the surface diffusion of such surface adatoms results in them reaching spots of actual contact, the oxidation reaction of these adatoms can take place and silver ions and electrons can be generated from the reaction.

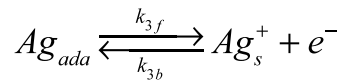
The rate constants associated with each of these processes can become rate limiting in different conditions. In the experimental conditions, however, the surface diffusion rate k₁ and incorporation rate k₄ are usually orders of magnitude higher than the rest. Therefore, the S4 etch rate is governed by k₃ and k₅, which are the adatom formation, silver oxidation, as well as ionic transport rates respectively. These rates are usually expressed as

$$k_1 \propto \exp\left(\frac{-E_A}{k_B T}\right) \dots\dots \text{Equation 3-7}$$

$$k_3 \propto \exp\left(\frac{nFV^0}{RT}\right) \dots\dots \text{Equation 3-8}$$

$$k_5 \propto \sigma_{Ag} \propto n \exp\left(\frac{-(h+u)}{k_B T}\right) \dots \dots \text{Equation 3-9}$$

where k_1 is the adatom formation rate, E_A is the activation energy for such process, k_3 is the silver oxidation rate, V^0 is the overpotential experienced by the silver atoms on the interface, k_5 is the transport rate of silver in silver sulfide. For reaction constant k_3 , consider the oxidation reaction at the Ag-Ag₂S interface



The electrical current density from the reaction can be expressed as

$$\frac{i_a}{nFA} = v_f = k_{3f} \cdot c_{ada}(0,t) \text{ for anodic direction flow, and}$$

$$\frac{i_c}{nFA} = v_b = k_{3b} \cdot c_{Ag_s^+}(0,t) \text{ for cathodic direction flow. The new current density is then}$$

the sum of the two and can be written as

$$i_{react} = i_a - i_c = nFA(v_f - v_b) = nFA \left[k_{3f} \cdot c_{ada}(0,t) - k_{3b} \cdot c_{Ag_s^+}(0,t) \right]$$

.....Equation 3-10

In the case of potentiostatic conditions and considering the $k_2, k_4 \gg k_1, k_3, k_5$ (activation energy for adatom diffusion ~ 0.1 eV, rate of silver incorporation into silver sulfide $\sim 10^{16}$ atoms/cm²s) [6-9], the total reaction current can be simplified to

$$i_{react} = nFA \left[k_{3f} \cdot c_{ada} - k_{3b} \cdot c_{Ag^+} (0, t) \right] \dots \text{Equation 3-11}$$

This expression states that the reaction component of the total current measured by the potentiostat is a function of the adatom concentration on the interface region, and the temporal profile of the silver ion concentration at the Ag-Ag₂S interface. The forward and backward reaction constants in equation 1 are a function of externally applied electrical potentials and can be analyzed in the following manner.

The free energies of anodic and cathodic reactions are of the form

$$\Delta G_a^* = \Delta G_{0a}^* - \beta F (V - V^0)$$

and

$$\Delta G_c^* = \Delta G_{0c}^* + (1 - \beta) F (V - V^0)$$

where ΔG_{0a}^* and ΔG_{0c}^* are the standard free energy at equilibrium, β is the transfer coefficient, and the term $(V - V^0)$ denotes the anodic overpotential. The rate constants are related to the free energies and can be expressed as

$$k_{3f} = A_f \exp\left(\frac{-\Delta G_{0a}^*}{RT}\right) \exp\left[\frac{-\beta F (V - V^0)}{RT}\right] \text{ for the forward reaction constant and}$$

$$k_{3b} = A_b \exp\left(\frac{-\Delta G_{0c}^*}{RT}\right) \exp\left[\frac{(1 - \beta) F (V - V^0)}{RT}\right] \text{ for the backward reaction constant}$$

Defining k^0 as the rate constant at equilibrium conditions, the forward and backward reaction constants can be simplified to

$$k_{3f} = k^0 \exp\left[\frac{-\beta F(V - V^0)}{RT}\right] \text{ and}$$

$$k_{3b} = k^0 \exp\left[\frac{(1 - \beta)F(V - V^0)}{RT}\right]$$

substituting these two expressions into equation 1, one can obtain the expression that describes the electrical current associated with the silver dissolution reaction on the interface.

$$i_{react} = nFAk^0 \left[c_{ada} \cdot e^{\frac{-\beta F(V - V^0)}{RT}} - c_{Ag^+}(0, t) \cdot e^{\frac{(1 - \beta)F(V - V^0)}{RT}} \right] \dots \text{Equation 3-}$$

12

In this expression, one can observe that reaction current is linearly proportional to the changes in the adatom concentration and the silver ion concentration at the interface. It also follows exponentially with the changes in the overpotential on the anodic surface. In addition, it also depicts the nature of the measured electrical current being a competition between the silver oxidation reaction and the removal of product silver ions away from the interface by the migration of those ions. Conceptually, it describes how the forward reaction rate can reach a balance with the removal of product ions away from the interface by transport and that the reaction current can reach a steady-state value. The

constant k^0 is typically in the range of $0.01 \sim 0.1 \text{ m/s}$ and β is typically 0.5. The adatom concentration c_{ada} is only a function of temperature when the composition of the metal surface is fixed. The last term, $c_{Ag^+}(0, t)$, in this equation is the concentration of silver ions at the interface. It is the term that couples the kinetics of silver dissolution reaction with the transport of silver in the silver sulfide domain.

Using the transport model developed earlier in this chapter to solve $c_{Ag^+}(0, t)$ for the temporal distribution of the concentration of silver ions at $x=0$ (1-D) or on the interface, one can examine the effect of physical properties of the system on the electrical current observed by the potentiostat during a stamping process. In [Figure 3-7\(A\)](#), one can see that relative differences between adatom concentration and intrinsic silver ion concentration has major effect on maximum value of the reaction current, but has little effect on how much it can increase within a given amount of time. Conceptually, the relative amount of these two terms determines the chemical potential available for the oxidation reaction to overcome its energy barrier, but does not have much effect on how the product silver ions from the reaction can be accommodated into the electrolyte domain. In [Figure 3-7\(B\)](#), one can see that the intrinsic concentration of silver ion in silver sulfide can influence the amount of ramping in reaction current in that the more intrinsic Ag ions in the domain means more room for concentration decrease and will result in more reaction current increase in a given amount of time. In [Figure 3-7\(C\)](#) and [\(D\)](#) one can see the two quantities have effect on ramping time constant of the reaction current, or the time constant for the S4 system to reach a steady state. The increase in overpotential can significantly increase i_{max} and shorten the time constant of which the steady state of the

system is reached, and faster diffusion (and mobility since the diffusivity and mobility of silver are related by the Einstein relation) can also give rise to a shorter time constant.

Conceptually, the forward reaction rate follows exponentially with anodic overpotential, and it is reflected in the reaction current increase. In addition the higher overpotential also means larger driving force for ion transport, and the system can reach steady-state faster. While the rate of transport of product silver away from the interface has much less effect on maximum current, the time constant to reach steady state can alter noticeably when the transport of silver ions is changed. The electrical potential effect is verified in our experimental results as shown in [Figure 3-8](#). The current ramps to a higher current as the applied voltage increases. At the same time, the ramping time constant decreases with higher voltage as predicted earlier in the discussion.

The effects of physical properties discussed here are also seen in experimental conditions. [Figure 3-9](#) shows the electrical current measurements of the stamping processes carried out with a stamp made from the “silver side” of a crystal and the “sulfur side” of the same crystal and the calculation results with the kinetics model developed here. Silver side of a crystal means the side of the crystal that is constant in contact with the silver pellet for ion source, and the sulfur side means the side of the crystal that is right next to the liquid sulfur in the furnace. The property difference between the two is that the silver side of a crystal has higher silver concentration and is usually close to the upper bound of the stoichiometry of silver sulfide, whereas the sulfur side is the opposite. One can observe that the use of a “sulfur side” stamp gives rise to larger ramping of current, shorter time constant, and higher maximum current, as shown by the circles, as compared to using a “silver side” stamp, shown by the squares. The two solid lines are plotted by the use of

the kinetics model. One can observed that this model captures the nature of the reaction current behavior and the nature of the interfacial kinetics of the Ag-Ag₂S system.

3.5 CONCLUSION

A transport model for mixed electronic-ionic conduction in silver sulfide is developed based on the electrophoretic conditions in the silver sulfide during a stamping process. This model captures the transport properties of the Ag-Ag₂S system and can be used for design and optimization of the S4 process. Also, this model can used to study metal-solid electrolyte systems of similar nature. A kinetics model is also developed based on the processes on a solid-solid electrolyte interface. This model captures the nature of two Ag-Ag₂S systems of different silver sulfide stoichiometry, and can be used to predict the current behavior of different stamps. The models developed here are not only useful for study of the S4 process and related solid-solid electrolyte systems, it can also find applications in study of electrode design in battery design.

3.6 FIGURES

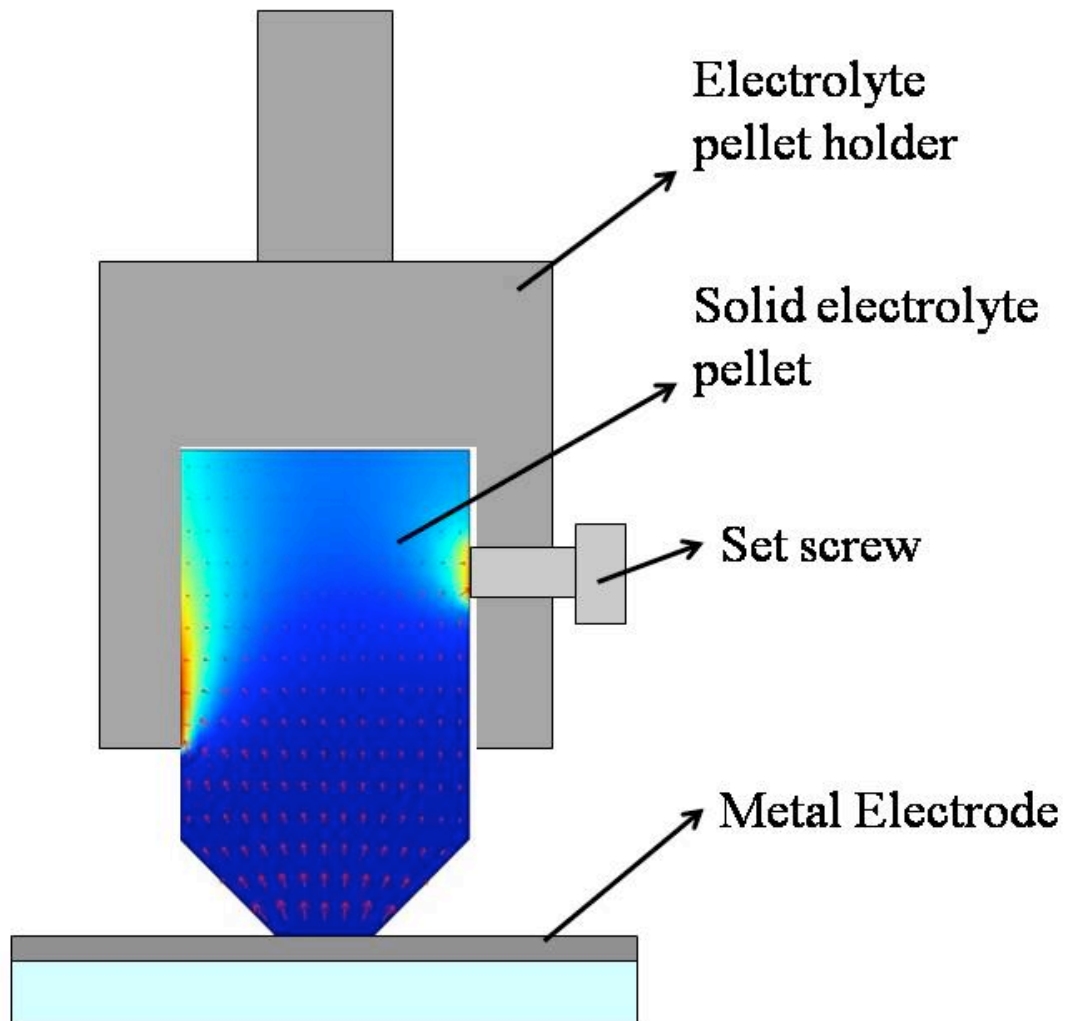


Figure 3.1 Experimental configuration of metal dissolution and transport in silver sulfide

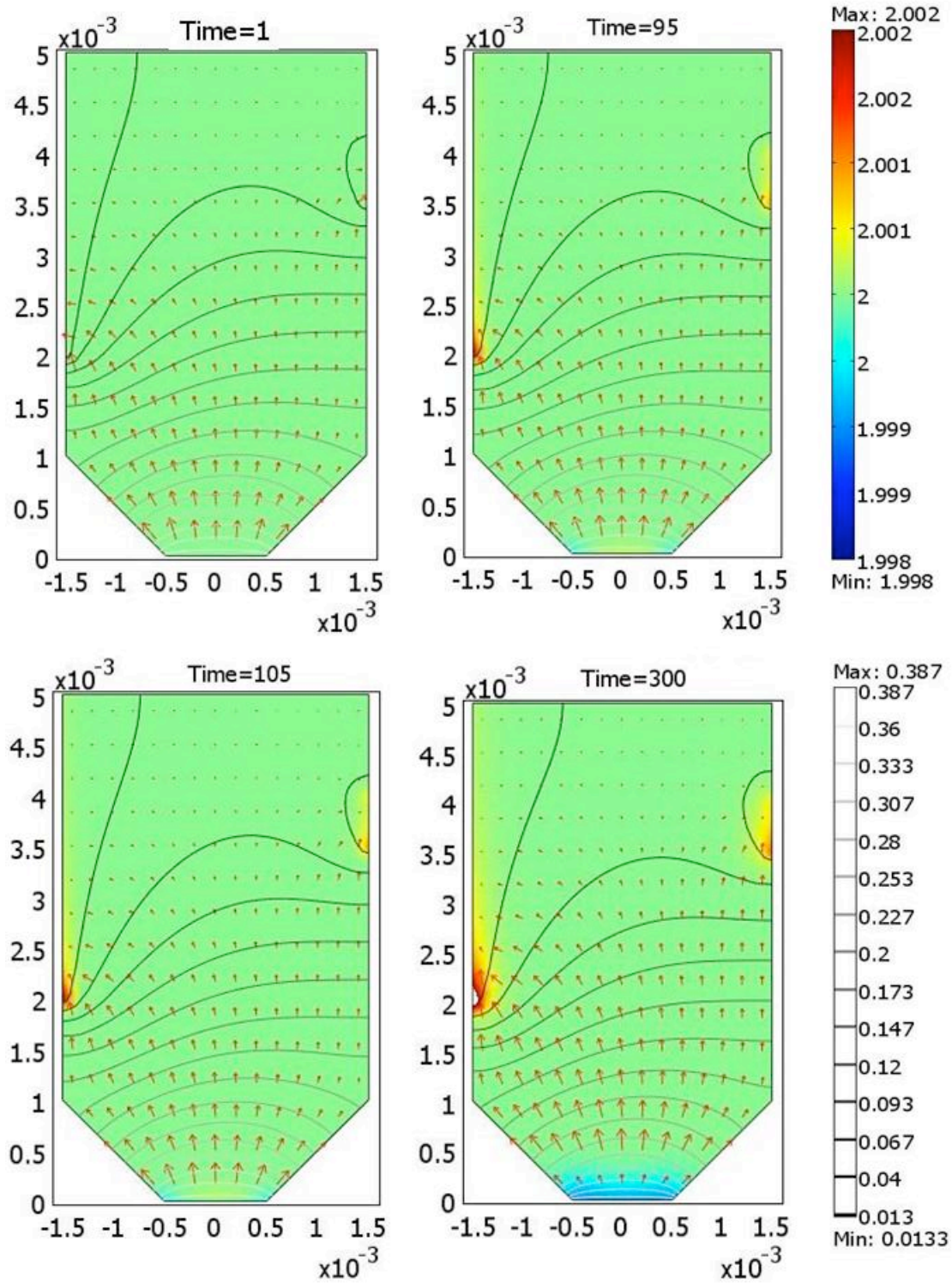


Figure 3.2 Temporal and spatial distribution of Stoichiometry, potential gradient, and total flux in silver sulfide

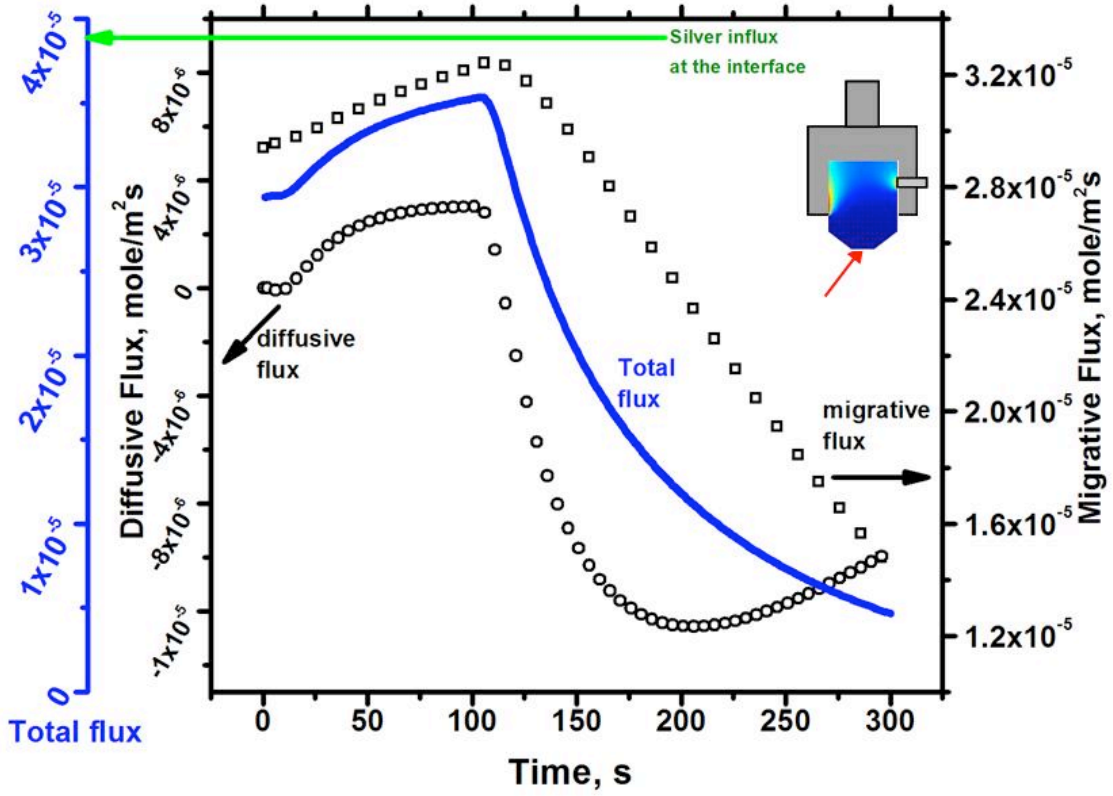


Figure 3.3 Temporal evolution of diffusive, migrative, and total flux at the interface

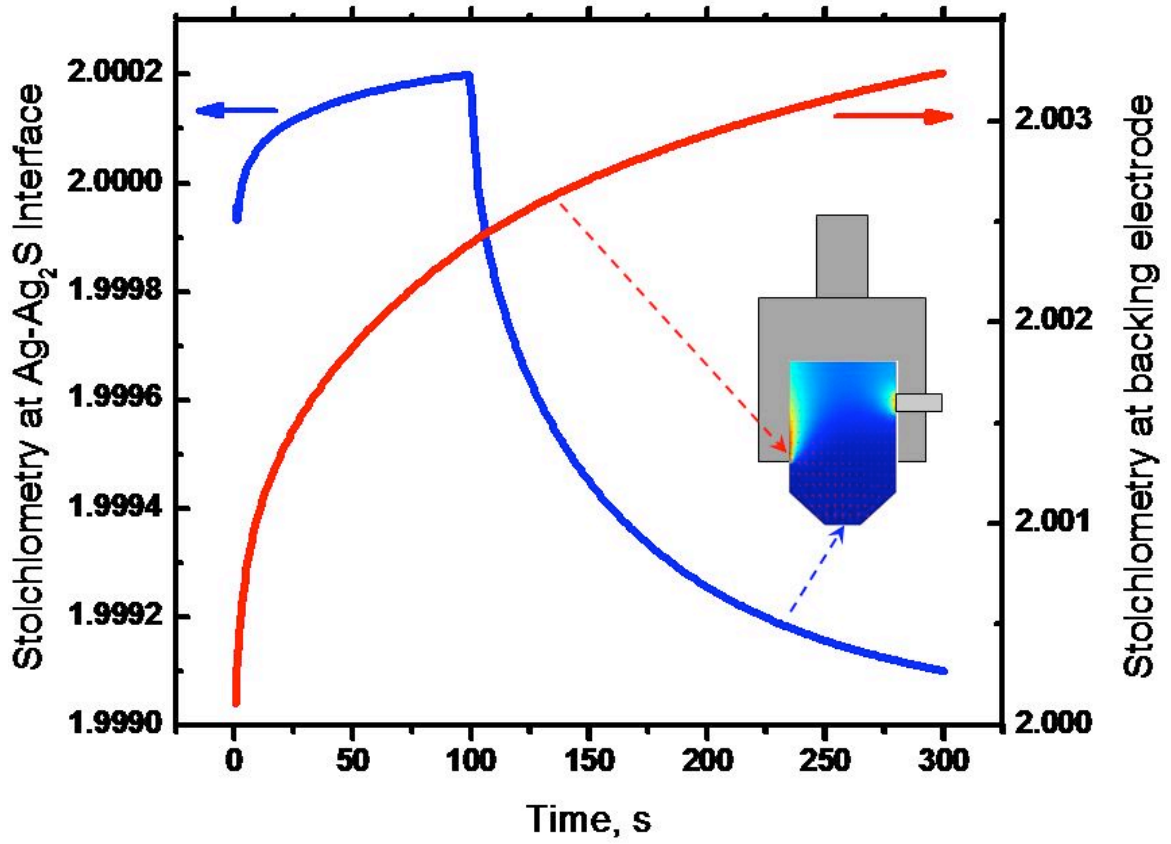


Figure 3.4 Temporal evolution of Stoichiometry at two interfaces

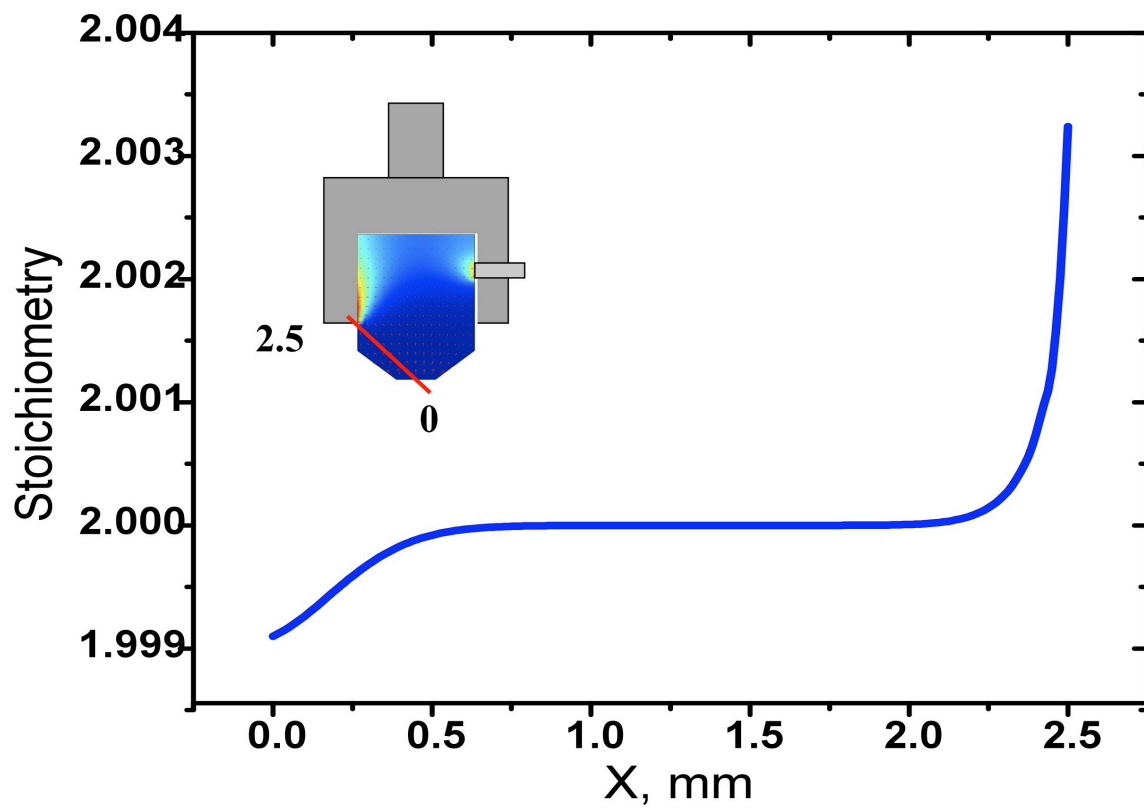


Figure 3.5 Spatial distribution of Stoichiometry in the electrolyte pellet

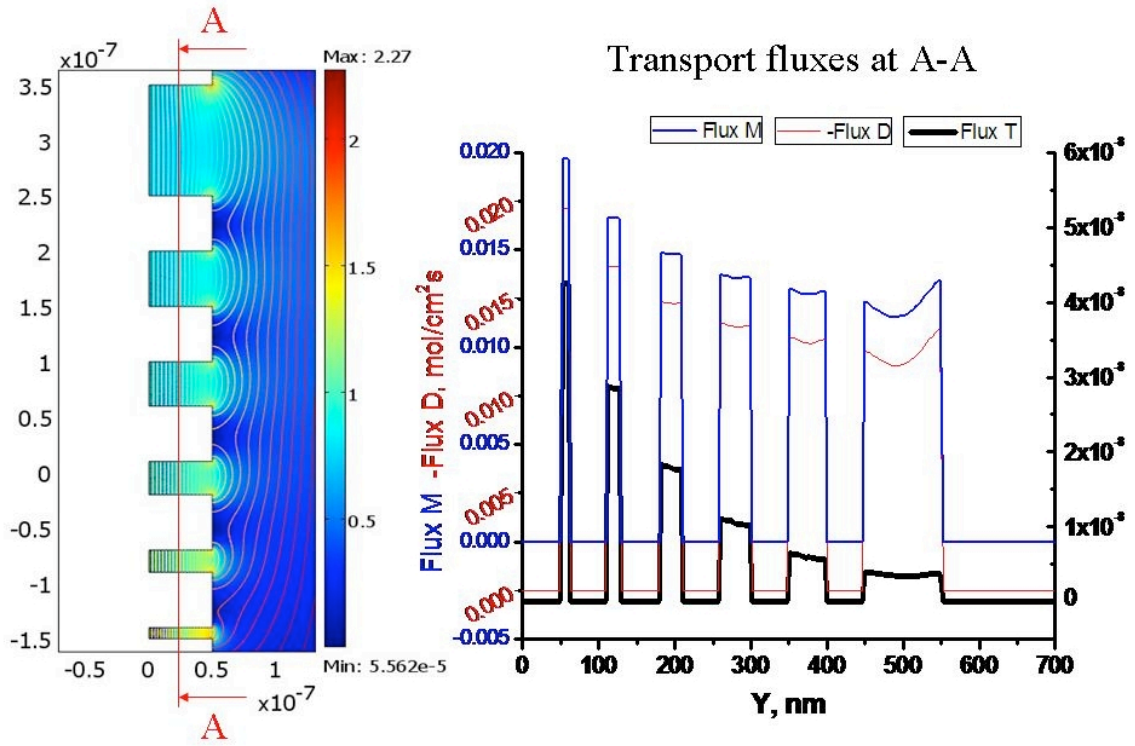


Figure 3.6 Feature size effect on transport properties

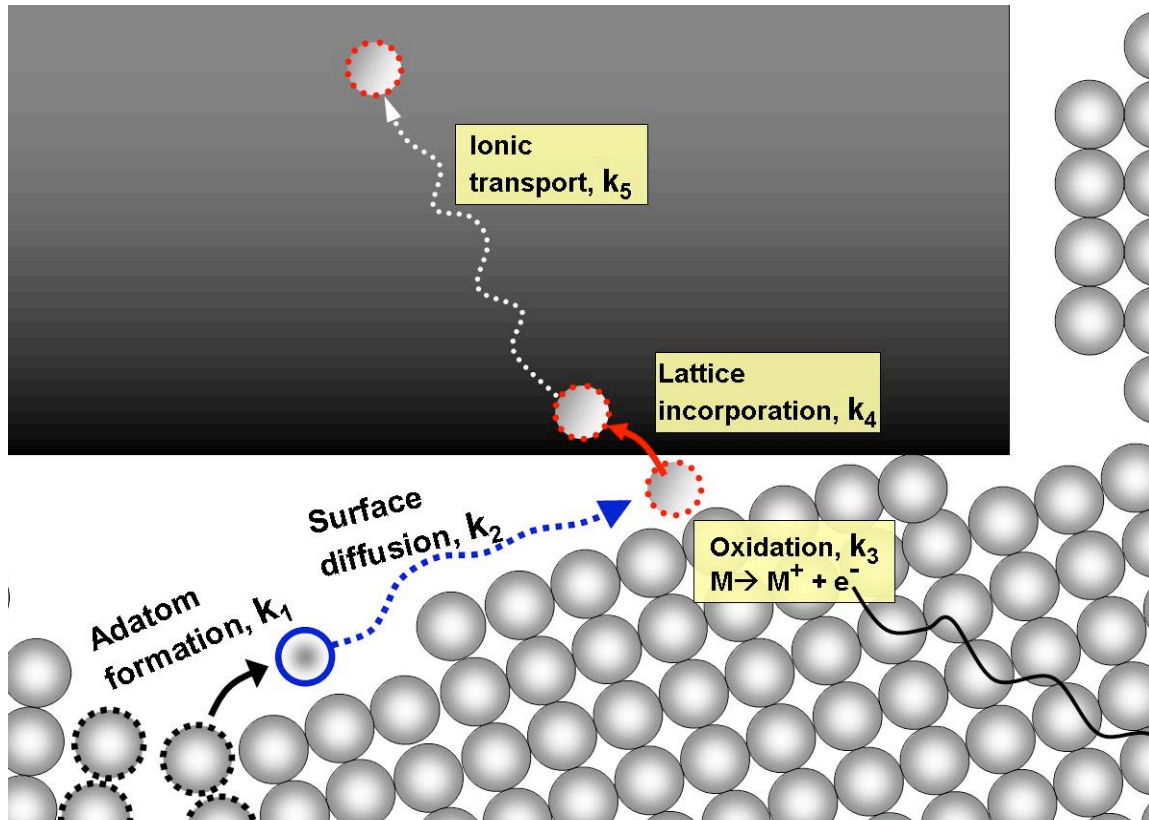


Figure 3.7 Interfacial processes on metal-solid electrolyte interfaces

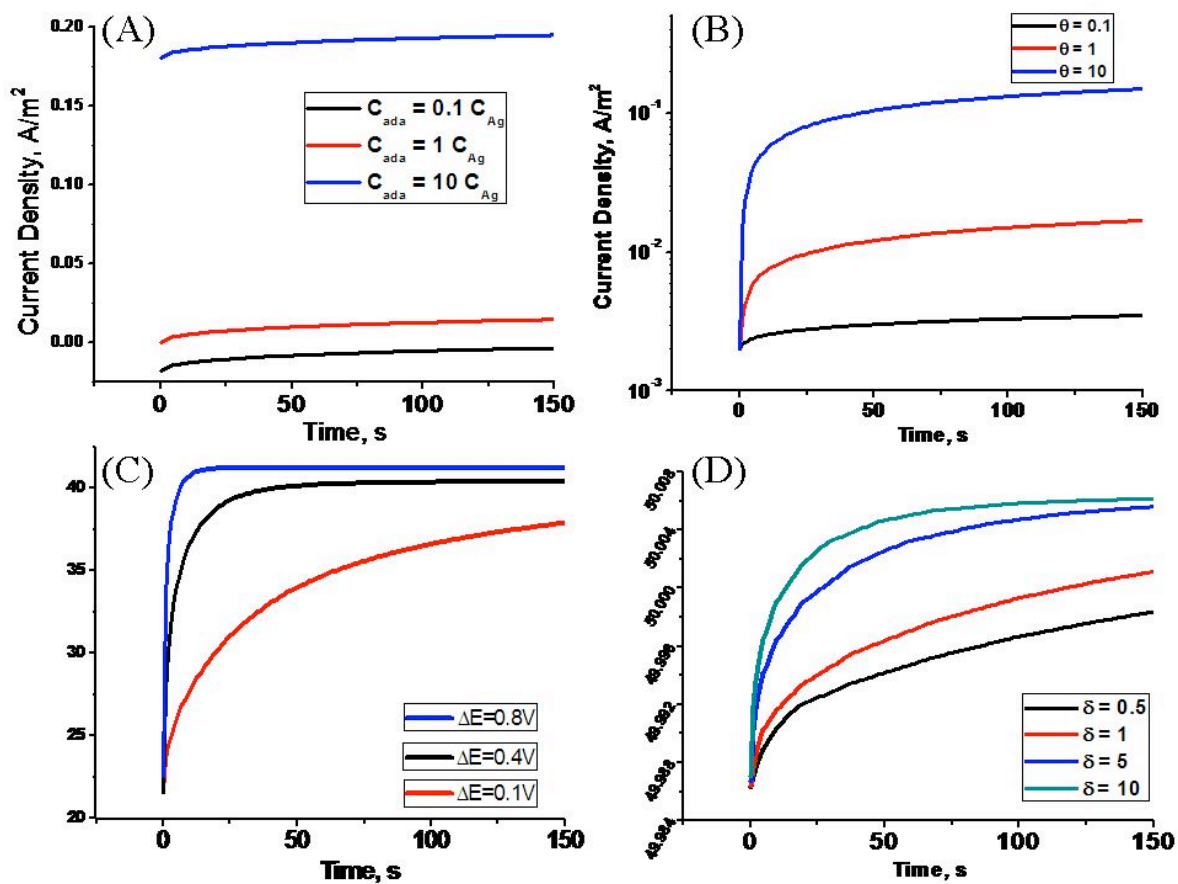


Figure 3.8 Parametric study of dynamic balancing between interfacial kinetics and ionic transport

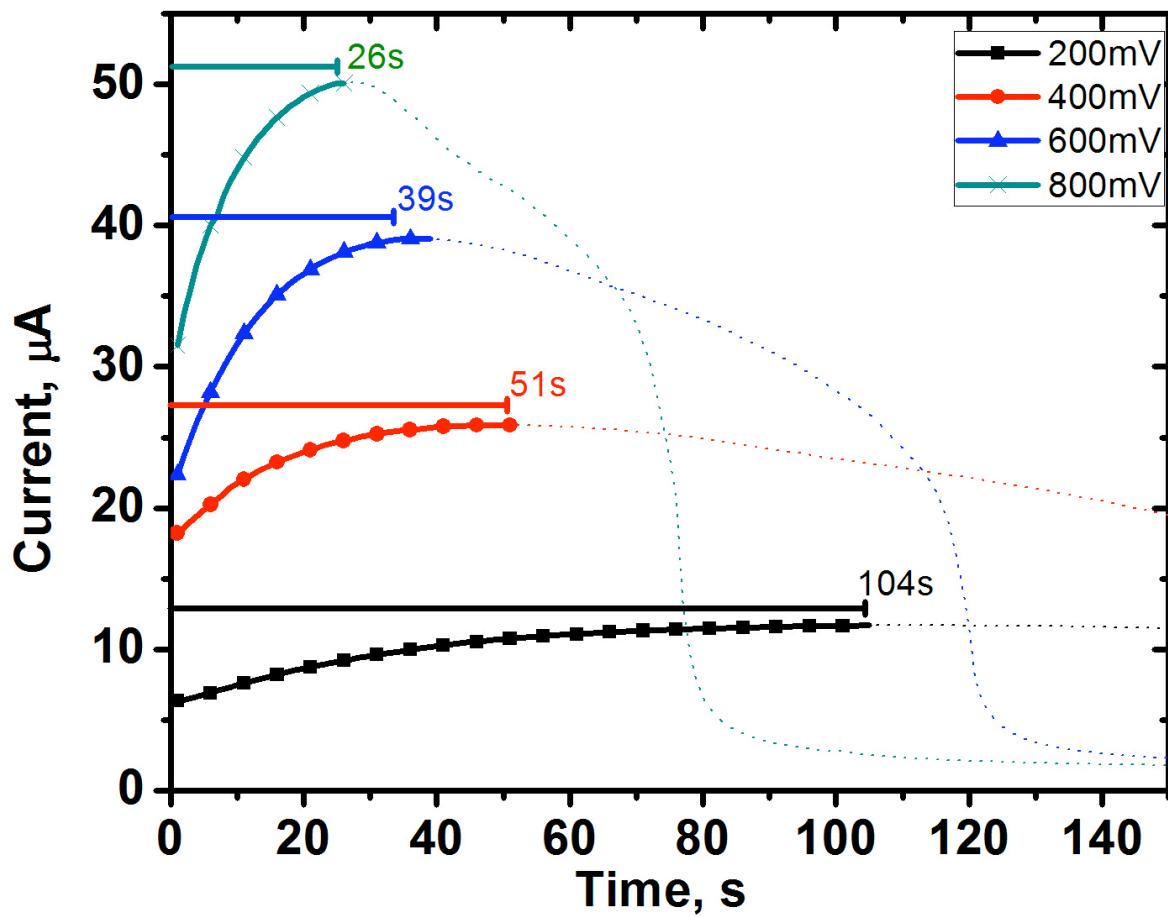


Figure 3.9 Current evolution at different applied potentials

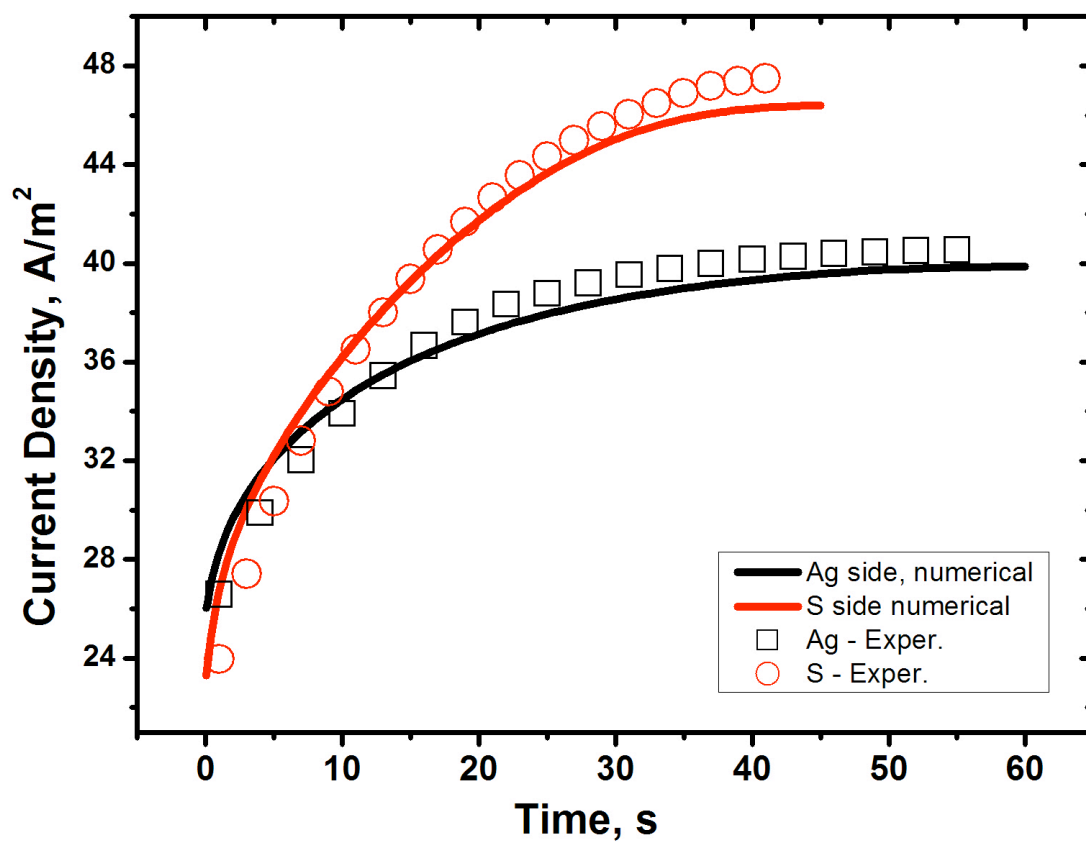


Figure 3.10 Dynamic balance between interfacial kinetics and ionic transport in solid electrolyte of two intrinsic states

3.7 TABLES

Table 3.1 List of constants and parameters for numerical modeling

| Constant | Value | Remarks | Remarks |
|-----------------|--|---|----------------|
| T | 25+273.15 | absolute temperature, K | |
| R | 8.3145 | universal gas constant (J/(mole*K)) | |
| D_ag | $1.4e-2 * \exp((-11100 * 4.18) / (R * T))$ | diffusivity of silver in silver sulfide, m ² /s | Ref. 1 |
| u_ag | D_ag/(R*T) | mobility of silver in silver sulfide, s.mol/kg | |
| R_et | R_et for 0<t<100, R_et from figure 2.XXX | silver ion influx boundary condition, mol/m ² .s | Note |
| c0 | 33.532 | intrinsic ion concentration, mole/m ³ | Note |
| Nav | 6.02E+23 | Avogadro's number | |
| k | 8.62E-05 | Boltzmann's Constant, eV/K | |
| epsilon | 8.8 | dielectric constant, Ag ₂ S | Ref. 3 |
| Vp | 0.4 | applied voltage, volt | |
| F | 96485.34 | Faraday's Constant | |
| sigma_e | 1.00E-01 | intrinsic electronic conductivity, S/m | Ref. 4 |

Note:

3.8 REFERENCE

1. V. Jovanovic and M. Jovanovic, The behavior of mixed metal sulfide/silver sulfide sensing materials in solutions of silver ions, *Ana. Chimica Acta*, 176, pp285-289, 1985
2. J. Han, Application of miniaturized electrochemical probes to nonisothermal transport studies in Ag₂S, *Solid State Ionics* 81, pp119-127, 1995
3. Ali Eftekhari, Chemical sensor based on silver / silver sulfide microelectrodes, *Analytical Letters*, 34, pp1087-1095, 2001
4. S. Miyatani, On the polarization of silver sulfide, *Journal of the Physical Society of Japan*, Vol. 10, No. 9, pp. 786-793, 1955
5. H. Kwon, U. Ravaioli, Simulation of electronic/ionic mixed conduction in solid ionic memory devices, *Microelectronics Journal*, 37, pp.1047-1051, 2006
6. John D. Porter, Timothy O. Robinson, Surface diffusion of silver at the silver (111)/liquid-water interface from electrocrystallization measurements, *J. Phys. Chem.*, 97 (25), pp 6696–6709, 1993

7. Papanicolaou N. I., Ecangelakis G. A., Kallinteris S. G., Molecular dynamics description of silver adatom diffusion on Ag(100) and Ag(111) surfaces, Computational materials science, vol. 10, no 1-4 pp. 105-110, 1998
8. Byung D. Y. and Matthias S., Ab initio study of step formation and self-diffusion on Ag (100), Physical Review B, Vol. 55, 13916-13924, 1997
9. J. Corish, M. T. Duffy and the late C. D. O'Briain, Electrochemical study of incorporation of silver vapour into -silver sulphide, Transactions of Faraday Society, 1971, 67, 1447 – 1452

CHAPTER 5.

INVESTIGATION OF LOCAL ELECTROMAGNETIC FIELD AGAINST FARFIELD SCATTERING IN THE CONTEXT OF PLASMON-ENHANCED RAMAN SCATTERING

5.1 INTRODUCTION

Since the first observation of the 6 orders of magnitude increase in the Raman signal of pyridine on roughened silver electrodes in the 1970s [1,2], the development in understanding of Surface Enhanced Raman Scattering, SERS, and in its application in fields such as material science, surface science, nanoscience has experienced dramatic growth [3-14]. Understanding the origin of such enhanced Raman scattering has been a quest since the finding of this phenomenon. It is generally recognized that the total 10^6 enhancement first observed is originated from a 10^2 chemical charge transfer enhancement and a 10^4 electromagnetic field enhancement. While researchers have thought that first arises from the excitation of adsorbate localized electronic resonance and is more or less limited to 100-fold, the latter is believed to be a result of Surface Plasmon Resonance on those coinage metal surface upon excitation. A line of research has since emerged to examine the EM-field enhancement of SERS. Topics examined include substrate with better defined substrates, applications to sensing, and single-molecule SERS [15-18].

In Raman spectroscopy, the treatment of SERS is often approximated as proportional to 4th power of local electromagnetic field, E. This approximation suggests that the ideal spectra location of LSPR for maximum EM-field enhancement is when it coincides with the excitation wavelength and the Raman shifted peak of interest. A recent study showed experimental agreement with this prediction where it was found that the highest SERS enhancement factor occurs when the excitation frequency was slightly higher than the LSPR frequency and lower than Raman shifted peak frequency[19-20]. Conventionally, the evaluation of LSPR is based on farfield extinction measurements where the intensity of a light beam passing through a substrate of interest is normalized to that of a reference beam of the same source. The “dip” on the transmission intensity spectrum is then attributed to the interaction of the light beam with the substrate and the generation of LSPR. Although a good measure of the substrate’s LSPR nature, it does not necessarily completely capture plasmon characteristics in the nearfield, especially when the local EM-field distribution is highly non-uniform. In such cases, the extinction is related to the local EM-field integration while the local EM-field maxima distribution affects SERS enhancement. The implication is that the nature of the nearfield behavior of a given substrate can be of equal, if not more, importance in terms of characterization of SERS enhancement as well as performance of SERS substrates.

In this letter, we examine this issue by characterizing the SERS of silver nano triangular features of various size, arrangement, and substrates. A novel solid-state electrochemical stamping technique introduced by Hsu et al. [21-23] was used to generate aforementioned substrate systems. As depicted in [Figure 5-1](#), this parallel process offers high reproducibility, pattern transfer fidelity, as well as flexibility in dimension and geometry

control and is ideal for generating large scale SERS features as well as prototyping SERS features for characterization.

5.2 EXPERIMENTAL

Two sets of samples are fabricated. Silver substrates were fabricated by vacuum evaporation of 40nm-thick silver with a 1nm-thick Cr adhesion layer on 170um-thick microscope cover slips at a pressure of 5×10^{-6} torr and followed by the solid-state electrochemical stamping technique introduced by Hsu et al. [21]. In this electrochemical stamping technique, silver sulfide stamp is carved with complementary hexagonal triangle array patterns of desired dimension by FIB. The stamp was then brought into contact with the silver thin-films fabricated earlier. Upon raising the potential of the silver film to 0.4V with respect to the reference electrode attached to the back of the stamp, the stamp progressively etched through the Ag film and formed the silver nanofeatures at a rate of about 1nm/s. We also fabricated with e-beam lithography bowtie arrays on Si substrates. As shown in [Figure 5-2](#), edge length of the triangles in the three arrays d is 120nm and the tip-to-tip spacing between the triangles g are 68nm, 133nm, and 170nm. In [Figure 5-2](#) the tip-to-edge height dimensions of the bowties are 120nm, 240nm, and 350nm, and the tip-to-tip spacing b is 20nm. Both sets of samples are conformably coated with 2.5nm Al_2O_3 by Atomic Layer Deposition (Cambridge NanoTech). The purpose for this inert Al_2O_3 layer is three fold. It prevents degradation of silver due to oxidation over time; it prevents chemical binding of examined molecules from forming a bonding to the silver surface and hence removes chemical charge transfer

enhancement; it also provides uniform adsorption to molecules to all surfaces coated with alumina including silver nanofeatures, blanket Ag film, and reference glass surface that will be used to characterize EF.

Far-field scattering spectra of the hexagonal triangle arrays were measured on an Axio Observer D1 inverted microscope (Carl Zeiss, Inc.) with a darkfield condenser lens. The spectra were collected with a UV-VIS spectrometer from Control Development, Inc. The condenser lens of 0.8NA, combined with a 20X objective, allows only light scattered from the substrate to be collected. The direct transmission from the substrate is eliminated. The farfield scattering spectra are a qualitative representation of the extinction spectra of the substrates.

1,1'-diethyl-2,2'-cyanine iodide ($C_{23}H_{23}IN_2$) molecules were used to examine the SERS effect of substrates fabricated. Substrates (each containing patterned region, un-altered Ag blanket film region, and reference glass region) were treated with the 2,2'-cyanine solutions by incubation in the solutions for 30 minutes to promote adsorption of the molecules to the alumina surface before rinsed with de-ionized water and followed by drying with nitrogen. As shown in [Figure 5-1](#), the Al_2O_3 layers were deposited with ALD which is shown to have very high uniformity. When doing the incubation, this insures the uniform adsorption of 2,2'-cyanine molecules to all surfaces that are coated with Al_2O_3 , including the silver nanofeature region, the SiO_2 region, as well as the Ag bulk film region.

Raman spectra were obtained on the Jobin Yvon LabRam HR 800 micro-Raman spectrometer with a 532nm laser excitation and a 100x objective. SERS signals of the

triangle arrays were collected by scanning mode when the laser beam spot ($\sim 1\mu\text{m}$ in diameter) rastered across the entire arrays and collective spectrum was recorded. SERS spectra of individual bowtie antennas were collected on Bruker Optics RamanScope III with a 532nm laser excitation and a 50X objective. The laser spot was focused down to about $5\mu\text{m}$ dia. [Figure 5-2](#) depicts the experimental configuration. Shown in [Figure 5-3](#) is the configuration of SERS measurements to study the effect of bowtie resonance on SERS enhancement. This sample system allows for simultaneous acquisition of the signature Raman peaks of the 2,2'-cyanine molecules adsorbed on the bowties (1350cm^{-1}) and the phonon Raman peak (520cm^{-1}) from the Si substrate the bowties reside on. Based on the two sets of spectra, the effect of substrate on Raman radiation directionality can be examined.

5.3 RESULTS AND DISCUSSION

5.3.1 Substrate effects on total Raman radiation

The notion that the SERS Enhancement factor can be correlated to a nanofeature's farfield extinction is based on correlation between the spectral and spatial characteristics of the local EM-field maxima and the farfield extinction of such nanofeature. However, such nearfield-farfield correlation is not always clear and straight forward. In simple geometries such as circular disks and single particle arrays whose spacing is relatively large (hence the interaction among the particles minimized), the nearfield and farfield correlation can be derived based on Optical Theorem, whereas when the nanofeature of consideration is more complex or the interaction among individual features needs to be

taken into account, the spectral characteristics of the local EM-field maxima is not necessarily related to the farfield extinction. In such cases, the SERS EF, which is due to the local EM-field enhancement, will relate to the spectral characteristics of local EM-field better.

An example of such correlation is shown in [Figure 5-4](#) where Raman scattering intensity of the cyanine dyes adsorbed on bowties of 120, 240, and 350nm were compared to the farfield extinction intensity as well as the local EM-field product(at the excitation and the 1350cm^{-1} Cyanine peak). Here one can clearly observe that the Raman intensity changes when the size of the bowtie changes is not reflected in the variations in the farfield extinction. Rather, the trend in Raman intensity change is clearly captured by the trend in the local EM-field maxima product. The reason lies in the fact that the farfield extinction is proportional to the integration of the local EM-field across the entire feature area and the total absorption of the feature; but the spectral characteristics of the local EM-field integration are not the same as those of the local EM-field maxima, or the “hot spots”. This is demonstrated in our calculation based on the 120nm bowtie shown in [Figure 5-5](#). Here the spectral peak of the local EM-field integration matches with the farfield extinction peak at around 750nm while the local EM-field at the “hot spot” is highest at 500nm. And it is those “hot spots” that contribute the most to the total Raman scattering. As such, since the farfield extinction is correlated to the local EM-field integration (given negligible absorption) and the SERS enhancement is proportional to the local EM-field maxima, the trend in SERS EF and trend in farfield extinction do not match, but follows the changes in the local EM-field maxima.

In addition to the spectral disagreement between the local EM-field maxima and farfield

extinction, the spatial distribution of them also plays a role in how the SERS EF is affected. Shown in [Figure 5-5](#) are the calculated extinction spectra as well as the local spatial distribution of EM-field along the cross-section of the bowties (120, 240, and 350nm in size) on silicon substrates. One can observe that at wavelength 547nm, the 350nm bowtie has the highest extinction efficiency as compared to the other two. However, the spatial distribution of the local EM-field shows that at 547nm, the local EM-field at the bowtie gap extends spatially further than that in the 350nm bowtie with similar maxima value. This implies that the 240nm bowtie has larger “hot spot” that can contribute more to SERS enhancement even though their farfield extinction says that the 350nm should give rise to higher enhancement.

The above discussion suggests that in simple geometry cases, sphere for example, where absorption cross-section of the system is also small as compared to its scattering cross-section, the spectral characteristics of the farfield extinction follow closely with those of the scattering cross-section (or integration of total scattering in all directions in the nearfield) as well as those of the local EM-field maxima, due to the fact that most of the available resonant modes are excited with any certain excitation. In these cases, the spectral characteristics of the local EM-field are closely related to the farfield extinction. As such, the spectral characteristics of the SERS EF from those features, since they follow those of the local-EM-field maxima, and the local EM-field integration, will be captured in the farfield extinction as well. Such conditions are seen in many examples [\[20, 24-25\]](#).

However, the above condition is not true when the complexity of the geometry increases and different modes of resonance develop. In these cases, the spectral, as well as spatial,

characteristics of the local EM-field maxima can deviate from those of the local EM-field integration. As such, they will be different from those of the farfield extinction as well. Therefore, in cases like this, the SERS EF cannot be directly related to farfield extinction. The bowtie antenna in our study shows a great example of such deviation.

5.3.2 Farfield scattering of array features and their local field enhancement

As discussed previously, the notion that matching of plasmonic resonance of SERS substrates with excitation and Raman scattering frequency leads to maximum EF is not always true. Here another example is presented. Hexagonal arrays of triangles with 125nm in edge length and 88nm, 133nm, and 170nm, in tip-to-tip spacing ([Figure 5-7a](#)) are fabricated to study the effect of their plasmonic resonance on their EM-field enhancement. Upon examined with darkfield polychromatic illumination, the three sets of triangle arrays emit light of blue, green, and yellow in color respectively as shown in [Figure 5-7b](#). The corresponding far-field scattering spectra with intensities normalized to their respective number of repeating units of hexagonally arranged triangles are also shown in [Figure 5-7c](#). The far-field scattering spectra were measured with darkfield illumination achieved by letting polychromatic excitation pass through a ring aperture before it passed through the substrate. In this manner, the direct transmission through the substrate is excluded from the objective collecting the signal, and only light that has scattered by the nanofeatures on the substrate was collected. Although not the exact extinction behavior of the pattern arrays, these spectra give a qualitative measure of the relative scattering power of these triangle arrays across the frequency ranged measured, or their plasmons resonance. Similar results were observed as in the single bowtie cases: the trend in SERS EF is captured by the local EM-field maxima, not the farfield

extinction.(Figure 5-8)

5.4 CONCLUSION

A new solid-state electrochemical patterning technique was applied to fabrication of high resolution silver bowties antennas and hexagonal arrays that are difficult for conventional lithographic techniques. These silver nanofeatures were used to investigate the relation among SERS EF, extinction, local EM-field maxima of the features. We found that spectral extinction property or the plasmonic resonance of a given SERS substrate alone is not sufficient for determining optimal EF; the number of points of high local EM-field, or “hot spots”, as well as the distribution of those high-field spots plays an equally, if not more, important role. These findings are vital to SERS substrate design and optimization.

5.5 FIGURES

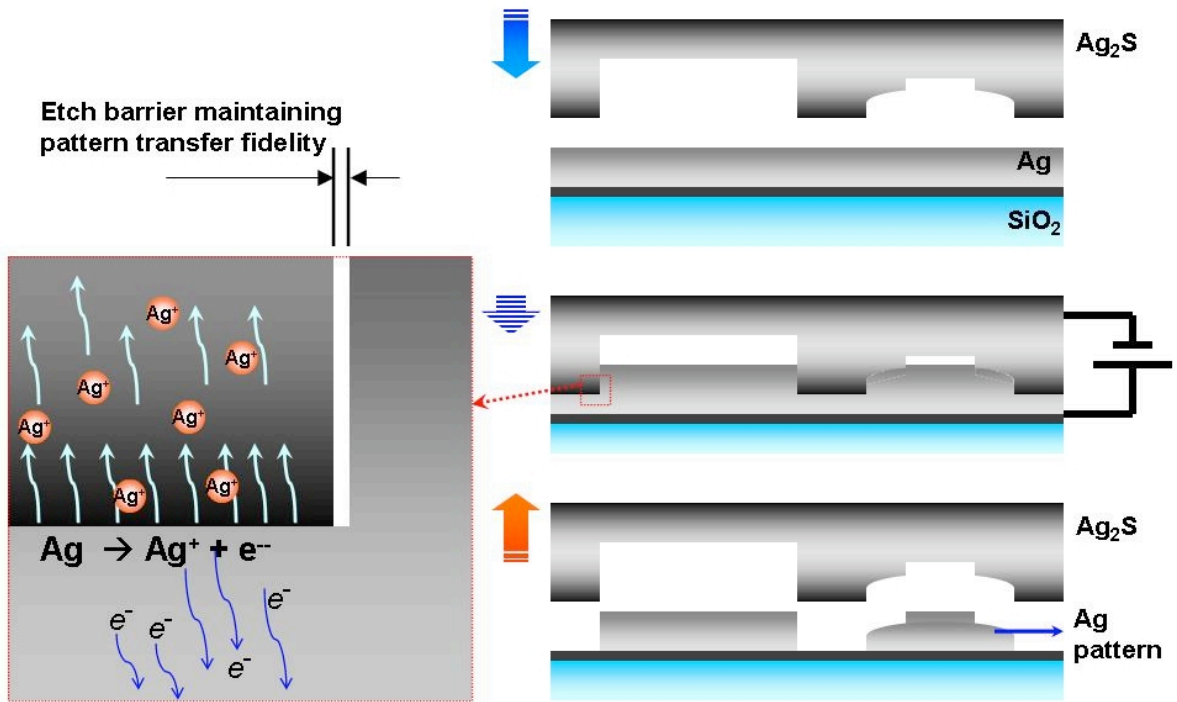


Figure 5.1 Solid State Superionic Stamping approach for fabrication of bowtie antennas

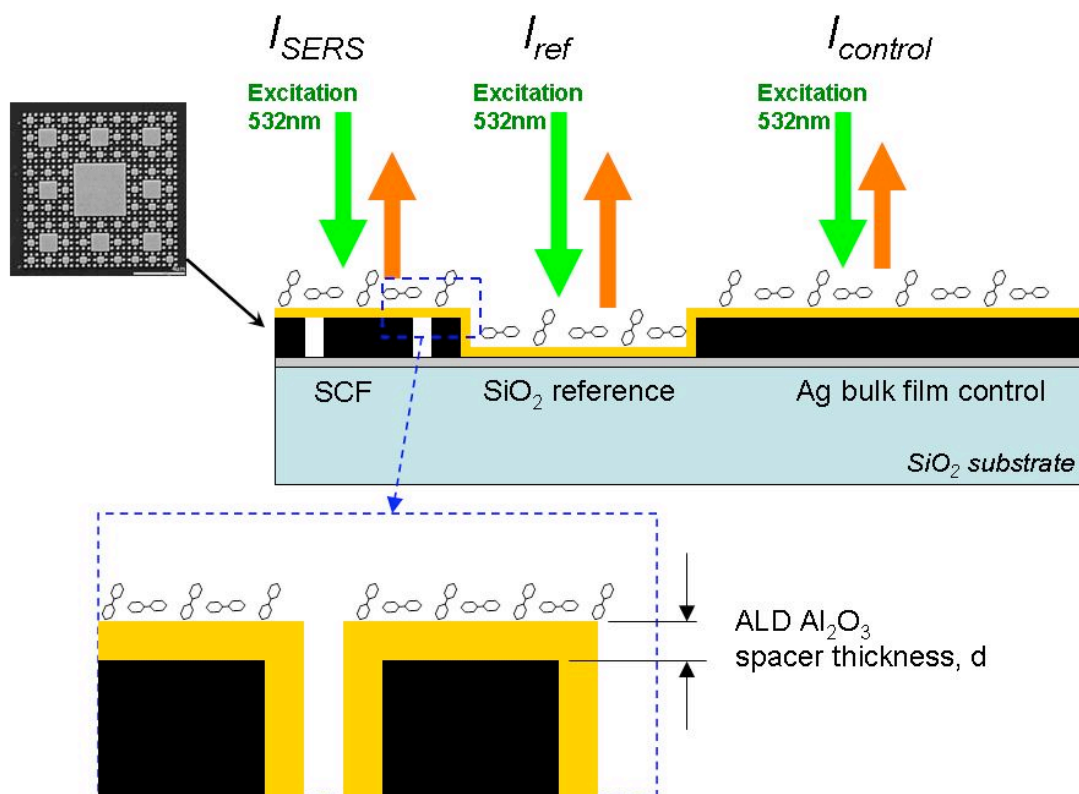


Figure 5.2 Sampling regions on S4-fabricated substrates and the use of uniform Atomic Layer Deposition Al_2O_3

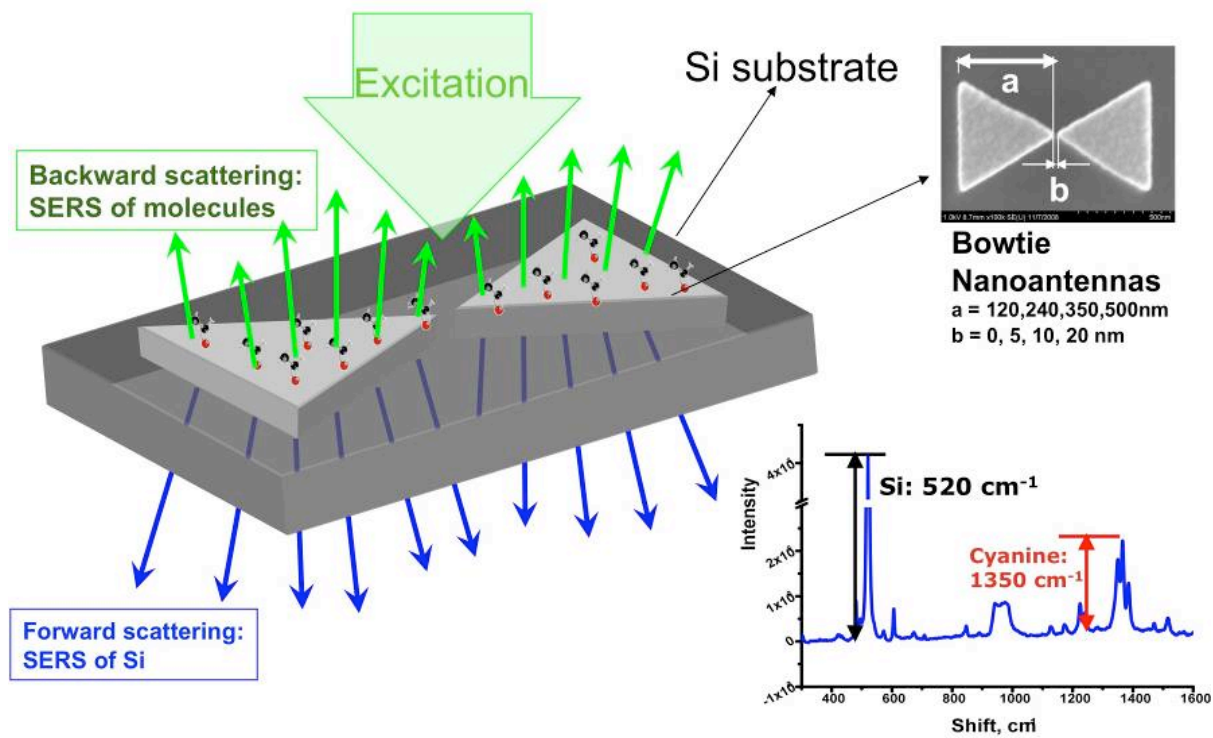


Figure 5.3 Configuration of excitation and signal collection

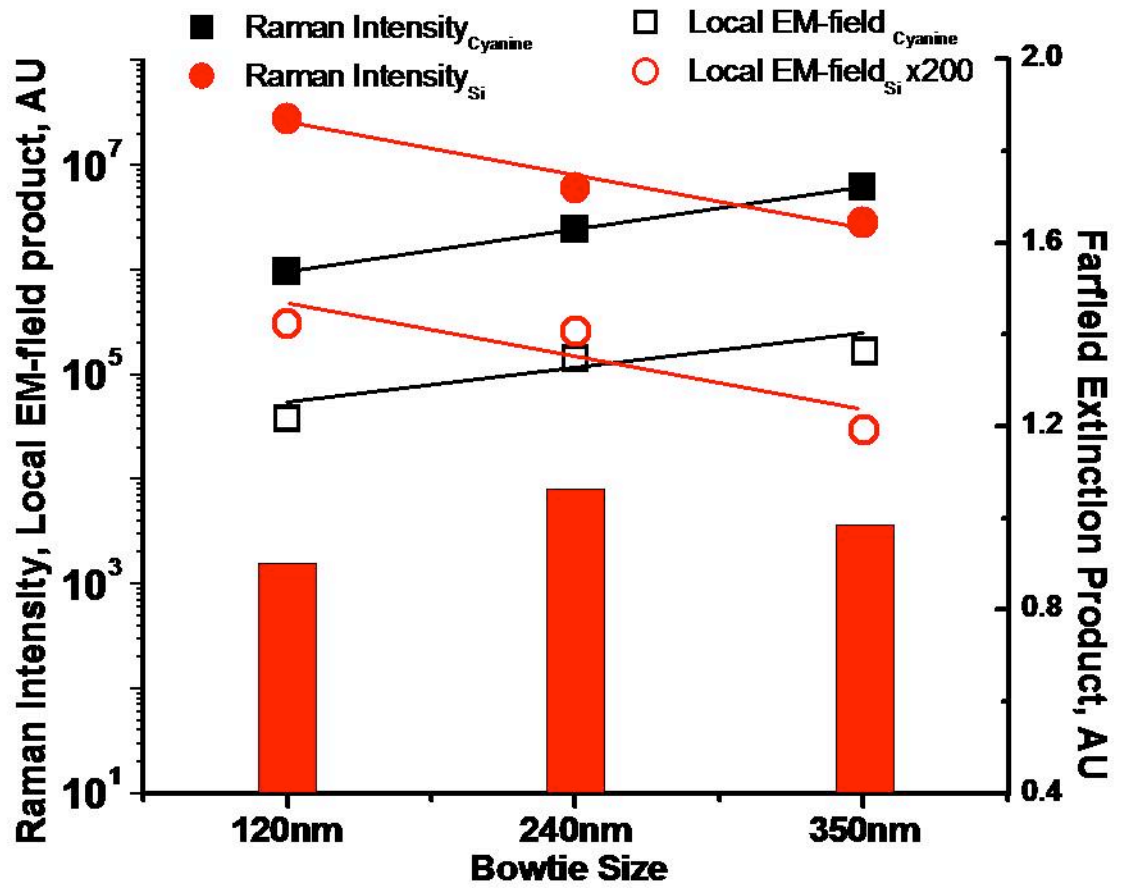


Figure 5.4 Match of local EM-field Maxima with SERS EM-field enhancement

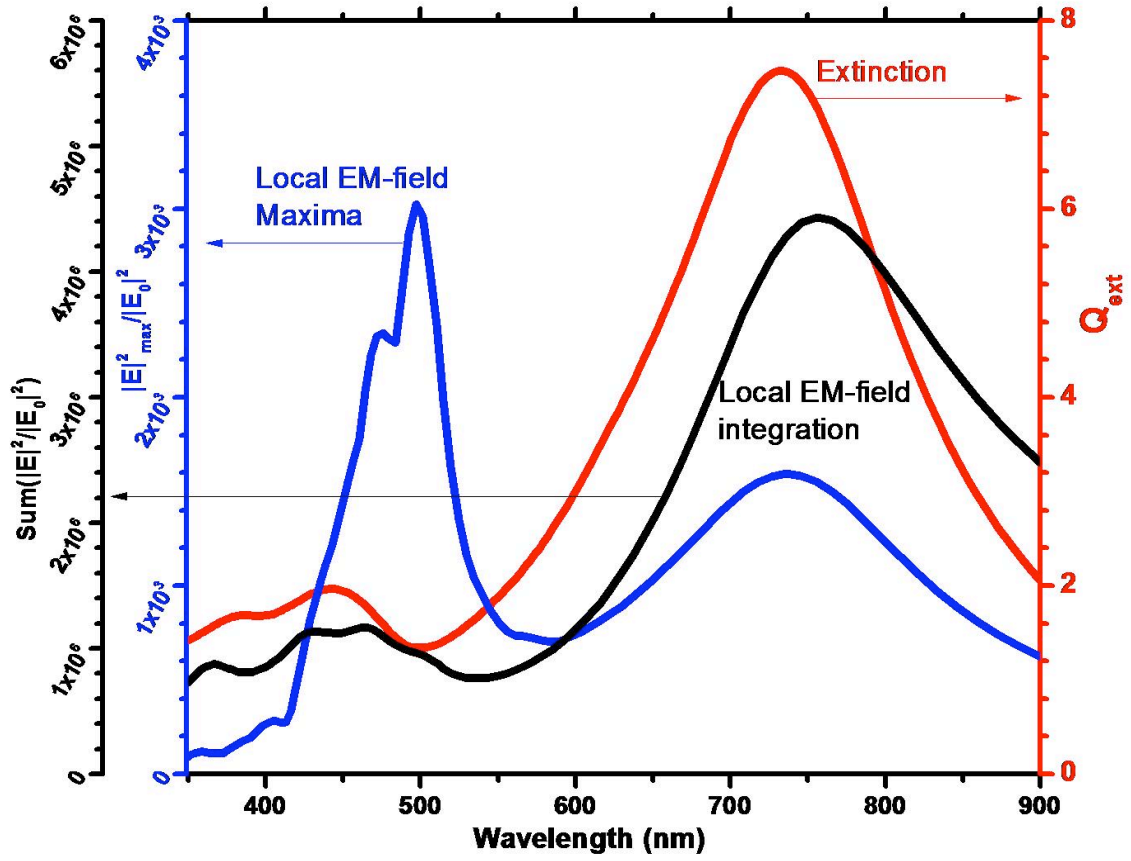


Figure 5.5 Spectral deviation of extinction and local EM-field maxima of a 120nm bowtie structure

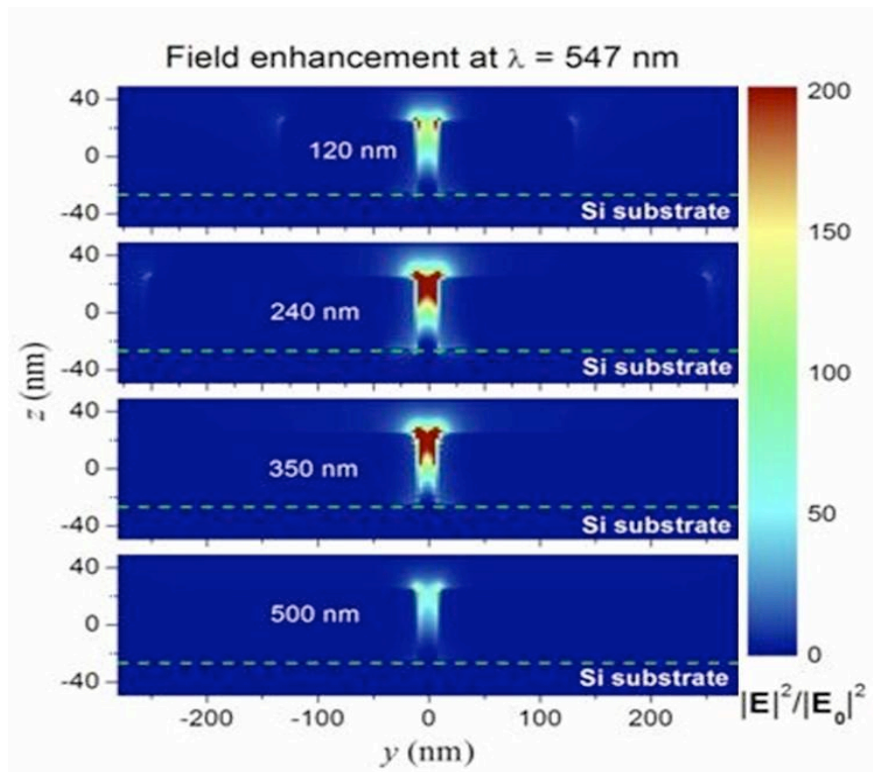
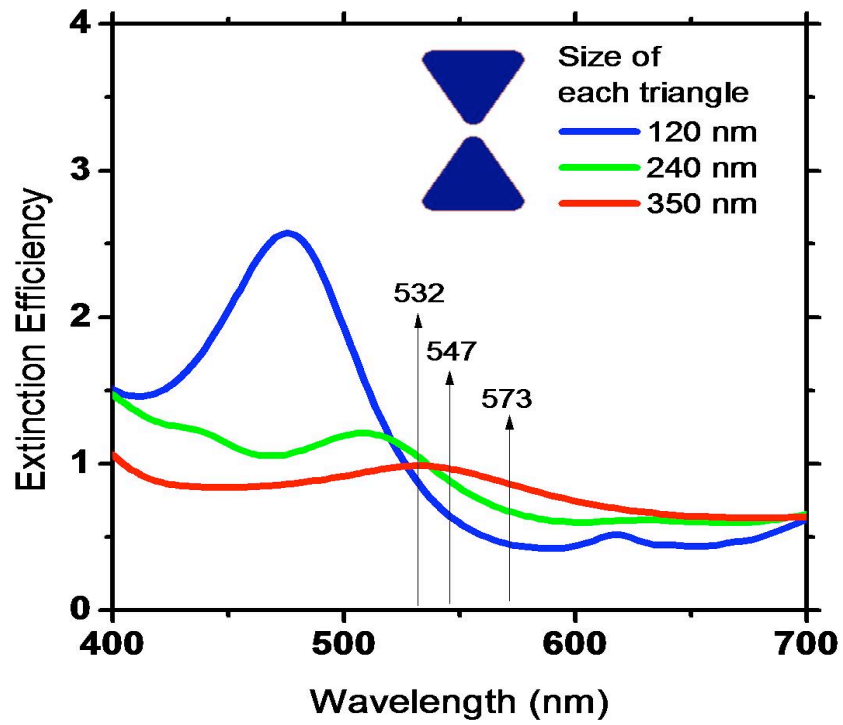


Figure 5.6 (a) Extinction spectra for bowties of various sizes (b) Local EM-field distribution on the vertical plane across the center of bowties

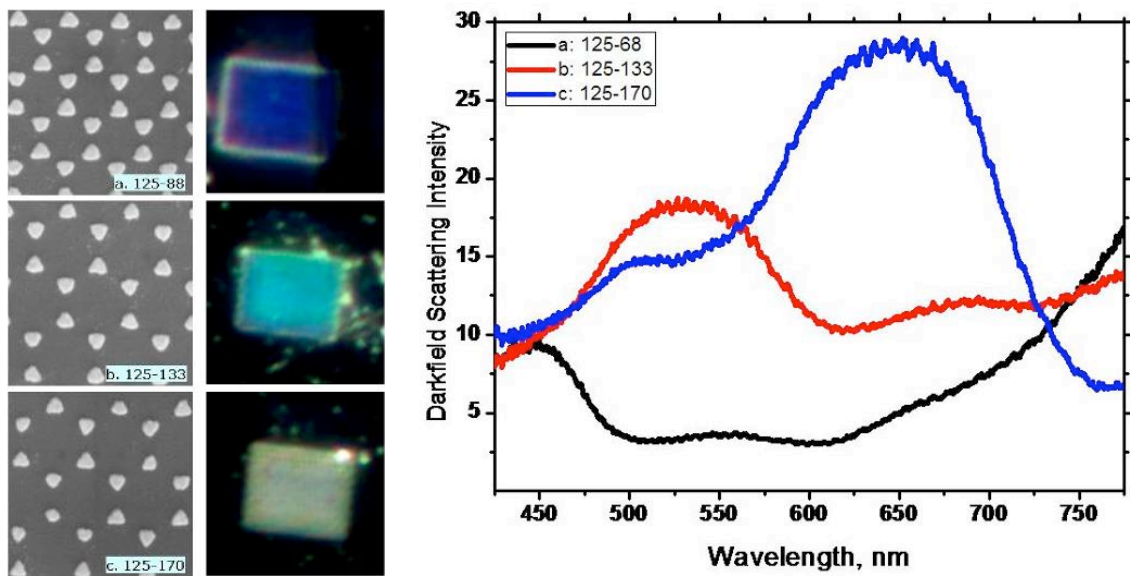


Figure 5.7 (a) Hexagonal triangle arrays (b) darkfield scattering image of the triangle arrays (c) Farfield scattering spectra of the triangle arrays with darkfield illumination

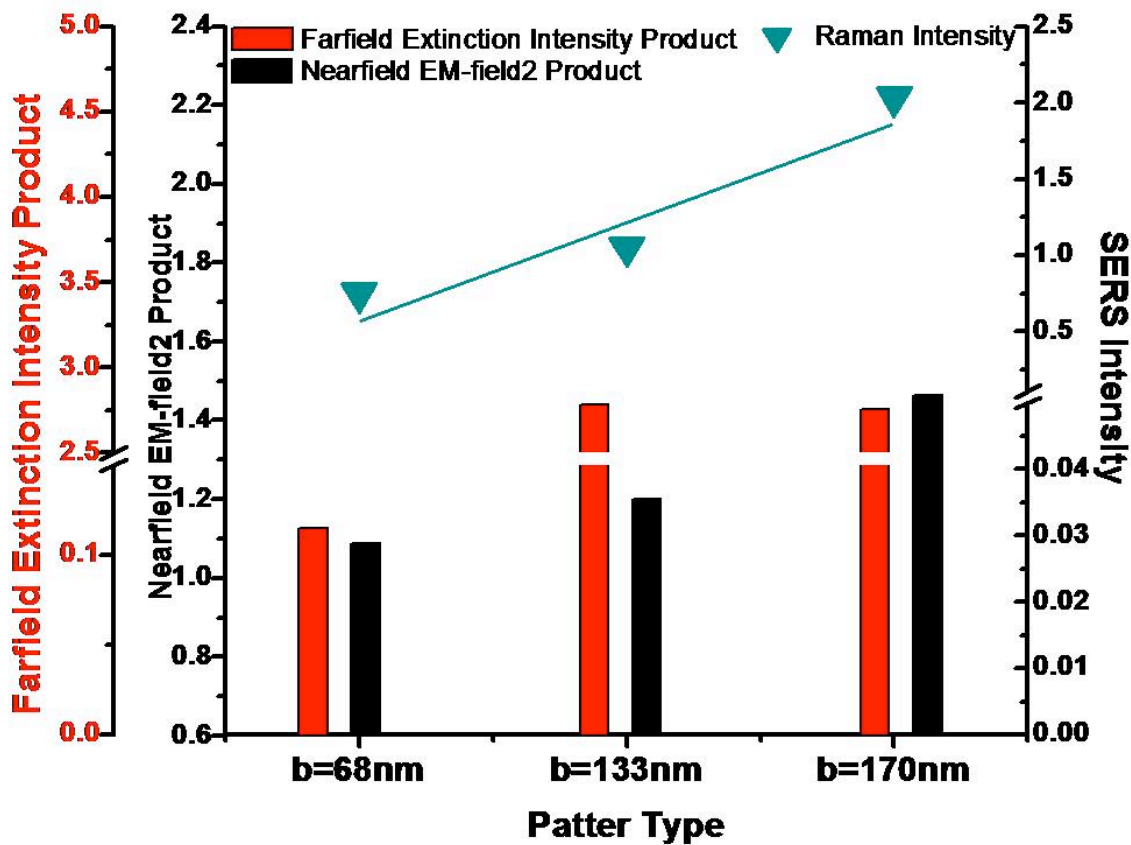


Figure 5.8 Comparison among darkfield extinction, SERS Enhancement, as well as calculated local EM-field maxima of hexagonal arrays of silver triangles on glass substrates

5.6 REFERENCE

1. Jeanmarie DL, Van Duyne RP. 1977. Surface Raman spectroelectrochemistry, part 1: heterocyclic, aromatic, and aliphatic amines adsorbed on the anodized silver electrode. *J. Electroanal. Chem.* 84:120
2. Albrecht MG, Creighton JA. 1977. Anomalously intense Raman spectra of pyridine at a silver electrode. *J. Am. Chem. Soc.* 99:5215–17
3. Campion A, Kambhampati P. 1998. Surface-enhanced Raman scattering. *Chem. Soc. Rev.* 27:241–50
4. Kneipp K, Kneipp H, Itzkan I, Dasari RR, Feld MS. 1999. Surface-enhanced Raman scattering: a new tool for biomedical spectroscopy. *Curr. Sci.* 77:915–24
5. Moskovits M. 1985. Surface-enhanced spectroscopy. *Rev. Mod. Phys.* 57:783–82
6. Stuart DA, Yonzon CR, Zhang XY, Lyandres O, Shah NC, et al. 2005. Glucose sensing using near-infrared surface-enhanced Raman spectroscopy: gold surfaces, 10-day stability, and improved accuracy.

Anal. Chem. 77:4013–19

7. Braun G, Pavel I, Morrill AR, Seferos DS, Bazan GC, et al. 2007. Chemically patterned microspheres for controlled nanoparticle assembly in the construction of SERS hot spots. *J. Am. Chem. Soc.* 129:7760–61
8. Braun G, Lee SJ, Dante M, Nguyen TQ, Moskovits M, Reich N. 2007. Surface-enhanced Raman spectroscopy for DNA detection by nanoparticle assembly onto smooth metal films. *J. Am. Chem. Soc.* 129:6378–79
9. Kneipp K, Kneipp H, Bohr HG. 2006. Single-molecule SERS spectroscopy. See Ref. 88, pp. 261–77
10. Willets KA, Van Duyne RP. 2007. Localized surface plasmon resonance spectroscopy and sensing. *Annu. Rev. Phys. Chem.* 58:267–97
11. Schatz GC, Young MA, Van Duyne RP. 2006. Electromagnetic mechanism of SERS. See Ref. 88, pp. 19–45
12. Chen LC, Ueda T, Sagisaka M, Hori H, Hiraoka K. 2007. Visible laser desorption/ionization mass spectrometry using gold nanorods. *J. Phys. Chem. C* 111:2409–15
13. Kneipp J. 2006. Nanosensors based on SERS for applications in living cells. See Ref. 88, pp. 335–49
14. Vo-Dinh T, Yan F, Wabuyele MB. 2006. Surface-enhanced Raman scattering for biomedical diagnostics and molecular imaging. See Ref. 88, pp. 409–26
15. Kerker M. 1984. Electromagnetic model for surface-enhanced Raman-scattering (SERS) on metal colloids. *Acc. Chem. Res.* 17:271–77
16. Metiu H, Das P. 1984. The electromagnetic theory of surface enhanced spectroscopy. *Annu. Rev. Phys. Chem.* 35:507–36
17. Moskovits M. 2005. Surface-enhanced Raman spectroscopy: a brief retrospective. *J. Raman Spectrosc.* 36:485–96
18. Nie SM, Emery SR. 1997. Probing single molecules and single nanoparticles by surface-enhanced Raman scattering. *Science* 275:1102–6
19. Haynes CL, Van Duyne RP. 2003. Plasmon-sampled surface-enhanced Raman excitation spectroscopy. *J. Phys. Chem. B* 107:7426–33
20. McFarland AD, Young MA, Dieringer JA, Van Duyne RP. 2005. Wavelength-scanned surface-enhanced Raman excitation spectroscopy. *J. Phys. Chem. B* 109:11279–85
21. Hsu, K.H., Schultz, P.L., Ferreira, P.M., and Fang, N.X, Electrochemical Nanoimprinting with Solid-State Superionic Stamps, *Nano Lett.*, 2007, Vol. 7 No. 2, 446-451.
22. Schultz P., Hsu, K., Fang, N., and Ferreira, P., *Journal of Vacuum Science & Technology B: Microelectronics and Nanometer Structures* -- November 2007 -- Volume 25, Issue 6, pp. 2419-2424

23. Hsu K. H., P. L. Schultz, N. X. Fang and P. M. Ferreira, Electrochemical Nanoimprinting of Silver and Copper with the Solid-State Superionic Stamping (S4) process, *Unconventional Patterning Techniques and Applications*, John Rogers and Hong H. Lee, eds, John Wiley and Sons, 2008
24. A. Baca, Tu Truong, Lee Cambea, J. Montgomery, S. Gray, J. Rogers, Molded plasmonic crystals for detecting and spatially imaging surface bound species by surface-enhanced Raman scattering, *Appl. Phys. Lett.* 94, 243109, 2009
25. M. Stewart, C. Anderton, L. Thompson, J. Maria, S. Gray, J. Rogers, R. Nuzzo, Nanostructured Plasmonic Sensors, *Chem. Rev.*, 108, 494-521, 2008